https://doi.org/10.5194/acp-2021-815
Preprint. Discussion started: 25 October 2021

Atmospheric Chemistry and Physics Discussions

MAX-DOAS observations of formaldehyde and nitrogen dioxide at three sites in Asia and comparison with the global chemistry transport model CHASER

Hossain M. S. Hoque[1], Kengo Sudo[1,2], Hitoshi Irie[3], Alessandro Damiani[3], and Al Mashroor Fatmi[3]

[1]Graduate School of Environmental Studies, Nagoya University, Nagoya, 4640064, Japan
[2]Japan Agency for Marine-Earth Science and Technology (JAMSTEC), Kanagawa, 2370061, Japan
[3]Center for Environmental Remote Sensing (CEReS), Chiba University, Chiba,2638522, Japan

Correspondence to: Hossain M. S. Hoque (hoque.hossain.mohammed.syedul@a.mbox.nagoya-u.ac.jp)

Abstract. Formaldehyde (HCHO) and nitrogen dioxide (NO_2) concentrations and profiles were retrieved from ground-based multi-axis differential optical absorption spectroscopy (MAX-DOAS) observation during January 2017 through December 2018 at three sites in Asia: (1) Phimai in Thailand (15.18°N, 102.5°E); (2) Pantnagar (29°N, 78.90°E) in the Indo Gangetic plain (IGP) in India; and (3) Chiba (35.62°N, 140.10°E) in Japan. The NO_2 and HCHO partial columns (<4 km) and profiles simulated using the global chemistry transport model (CTM) and CHASER were compared to those of MAX-DOAS. The vertical sensitivity of the datasets was elucidated using the averaging kernel (AK) information from the MAX-DOAS retrievals. The NO_2 and HCHO concentrations at all three sites showed consistent seasonal variation throughout the investigated period. Biomass burning affected the HCHO and NO_2 variation in Phimai during the dry season and in Pantnagar during spring (March-May) and the post-monsoon (September-November) season. High NO_2 concentrations in Phimai during the wet season (June-September) are attributed to soil emissions of nitrogen oxides (NO_x), confirmed from satellite observations and CHASER simulations. Comparison with CHASER shows that the seasonal variations in the HCHO and NO_2 abundances at Phimai and Chiba agree well, with a correlation coefficient (R) of 0.80. Results agree with the variation, ranging mainly within the one sigma standard deviation of the observations. At Phimai, pyrogenic emissions contribute to the HCHO and NO_2 concentrations up to ~

https://doi.org/10.5194/acp-2021-815
Preprint. Discussion started: 25 October 2021


Atmospheric Chemistry and Physics Discussions

50 and ~35%, respectively. CHASER showed limited skills in reproducing the NO_2 and HCHO variability at Pantnagar. However, the CHASER simulations in the IGP region showed good agreement with reported results. Sensitivity studies showed that anthropogenic emissions affected the seasonal variation of NO_2 and HCHO concentrations in the IGP region.

1 Introduction

Formaldehyde (HCHO) is the most abundant carbonyl compound in the atmosphere because it is a high-yield product of oxidization of all primary volatile organic carbons (VOCs) emitted from natural and anthropogenic sources by hydroxyl radicals (OH). Oxidization of long-lived VOCs such as methane produces a global HCHO background concentration of 0.2–1.0 ppbv in remote marine environments (Weller et al., 2000; Burkert et al., 2001; Singh et al., 2004; Sinreich et al., 2005). Aside from oxidization of VOCs, the primary emission sources of HCHO are direct emission from biomass burning, industrial processes, fossil fuel combustion (Lee et al., 1997; Hak et al., 2005; Fu et al., 2008;), and vegetation (Seco et al., 2007). However, oxidization of non-methane VOCs emitted from biogenic (e.g. isoprene) or anthropogenic (e.g. butene) sources govern the spatial variability of HCHO on a global scale (Franco et al., 2015). The sinks of HCHO include photolysis at wavelengths below 400 nm, oxidization by OH, and wet deposition, thereby limiting their life to a few hours (Arlander et al., 1995).

Nitrogen dioxide (NO_2), a key and an important atmospheric constituent, (1) participates in the catalytic formation of tropospheric ozone (O_3), (2) acts as a catalyst for stratospheric O_3 destruction (Crutzen, 1970), (3) contributes to the formation of aerosols (Jang and Kamens, 2001), (4) acts as a precursor of acid rain (Seinfeld and Pandis, 1998), and (5) strongly affects radiative forcing (Lelieved et al., 2002; Solomon et al. 1999). Nitrogen oxides (NO_x = NO (nitric oxide) + NO_2) are emitted from natural and anthropogenic sources. Primary NO_x emission sources are biomass burning, fossil fuel combustion, soil emissions, and lightning (Bond et al., 2001; Zhang et al., 2003). Actually, NO_x emissions degrade air quality. For that reason, they are listed as a leading air pollutant with global and national ambient air quality standards (Ma et al., 2013). Both HCHO and NO_2 are important intermediates in the global VOC–HO_x (hydrogen oxides)–NO_x catalytic cycle, which governs the O_3 chemistry in the troposphere (Lee et al., 1997; Houweling et al., 1998; Kanakidou et al., 2005; Hak et al., 2005). Consequently, both trace gases play crucially important roles in tropospheric chemistry.

https://doi.org/10.5194/acp-2021-815
Preprint. Discussion started: 25 October 2021


Atmospheric Chemistry and Physics Discussions

The working principle of multi-axis differential optical absorption spectroscopy (MAX-DOAS), a well-established remote sensing method for measuring trace gases and aerosols, is based on the DOAS technique. Aerosols and trace gases are quantified with analysis of selective narrowband (high frequency) absorption features (Platt 1994, Platt and Stutz 2008). Spectral radiation measurements taken at different elevation angles (ELs) can provide profile information of atmospheric trace gases and aerosols (Hönninger et al., 2004; Wagner et al., 2004; Wittrock et al., 2004; Frieß et al., 2006; Irie et al., 2008a). Many studies have demonstrated the retrieval of aerosol and trace gas concentrations and profiles from MAX-DOAS observations, including the respective concentrations of NO_2 and HCHO (Clemmer et al., 2010; Irie et al., 2011; Hendrick et al., 2014; Franco et al., 2015; Frieß et al., 2016; Wang et al., 2014).

The ability of MAX-DOAS to provide information related to surface concentrations, vertical profiles, and column densities makes it complementary to ground-based in situ and satellite observations. Moreover, the MAX-DOAS method uses narrowband absorption of the target compounds, thereby obviating radiometric calibration of the instrument. Because of these advantages, MAX-DOAS systems are deployed for assessment of aerosol and trace gases in regional and global observational networks such as BREDOM (Wittrock et al., 2004), BIRA-IASB (Clemer et al., 2010), and MADRAS (Kanaya et al., 2014). Such datasets are used in, but are not limited to (1) air quality assessment and monitoring, (2) evaluation of chemistry–transport models (CTMS), and (3) validation of satellite retrieval. Several studies have used MAX-DOAS datasets to validate tropospheric columns retrieved from satellite observations, including those of NO_2 and HCHO (; Ma et al., 2013; Irie et al., 2008b; Chan et al., 2020; Ryan et al., 2020). However, limited MAX-DOAS datasets have been used to evaluate global CTMs. Vigouroux et al. (2009) and Franco et al. (2015) respectively used the MAX-DOAS HCHO datasets from Reunion Island and Jungfraujoch stations to evaluate the Intermediate Model of Annual and Global Evolution of Species (IMAGES) and GEOS-Chem model simulations. Kanaya et al. (2014) validated the Model for Interdisciplinary Research on Climate–Earth System Model – Chemistry (MIROC-ESM-CHEM) simulated NO_2 column densities using MAX-DOAS observations in Cape Hedo and Fukue in Japan.

For this study, NO_2 and HCHO profiles retrieved from MAX-DOAS observations at the A-SKY (International air quality and sky research remote sensing) (http://atmos3.cr.chiba-u.jp/a-sky/) network sites are used to evaluate the global Chemical Atmospheric General Circulation Model for the Study of

https://doi.org/10.5194/acp-2021-815
Preprint. Discussion started: 25 October 2021

Atmospheric Chemistry and Physics Discussions

Atmospheric Environment and Radiative Forcing (CTM CHASER; Sudo et al., 2002). The three A-SKY sites of (1) Phimai in Thailand (15.18°N, 102.56°E), (2) Pantnagar (29°N, 78.90°E) in the Indo Gangetic plain (IGP) in India, and (3) Chiba (35.62°N, 140.10°E) in Japan respectively represent rural, semi-rural, and urban environments. CHASER has been used mostly for global-scale research (Sudo et al., 2007; Sekiya et al., 2014, 2018; Miyazaki et al., 2017). This report is the first of the literature to describe an attempt to evaluate the CHASER-simulated NO_2 and HCHO profiles using MAX-DOAS observations in three atmospheric environments. Moreover, no report of the relevant literature has described the use of MAX-DOAS datasets to evaluate global CTMs in southern and southeastern Asian regions. Consequently, this study was conducted to provide important insights into the model performances and to help reduce model uncertainties related to NO_2 and HCHO simulations in these regions.

The manuscript has been compiled in the following manner. The observation sites, MAX-DOAS instrumentation, and retrieval strategies are described in section 2. Section 2 also includes a short description of the CHASER model. Results obtained from the MAX-DOAS observations and the comparison between MAX-DOAS and CHASER datasets are presented respectively in sections 3.1 and 3.2. Section 4 presents concluding remarks.

2 Observations, datasets, and methods

2.1 Site Information

Continuous MAX-DOAS observations at Phimai, Pantnagar, and Chiba started respectively in 2014, 2017, and 2012. The MAX-DOAS observations for the two years from January 2017 through December 2018 at all three sites are discussed here. Phimai, a rural site, is ~260 km northeast of the Bangkok metropolitan region. Consequently, the Phimai site is unlikely to be affected by vehicular and industrial emissions. The site is, however, affected by two major air streams: the dry, cool northeast monsoon during November – mid-February and the wet, warm southwest monsoon during mid-May – September.

https://doi.org/10.5194/acp-2021-815
Preprint. Discussion started: 25 October 2021


Atmospheric Chemistry and Physics Discussions

Pantnagar, a semi-urban site in India, is located in the Indo-Gangetic Plain region (IGP). The Indian capital of New Delhi is located at ~225 km southwest of the site. The low-altitude plains are in the south and west directions, whereas the Himalayan mountains are located north and east of the site. An important roadway with moderate traffic volume and a small local airport lies within 3 km of the site. Rudrapur (~. 12 km southwest of Pantnagar) and Haldwani (~. 25 km northeast of Pantnagar) are the two major cities near Pantnagar; a few small-scale industries are established there. Climate classification in Pantnagar is the following: (1) winter (December–February), (2) spring (March–May), (3) summer monsoon (June–August), and (4) autumn (September–November).

Chiba, an urban site, is ~. 40 km southeast of the Tokyo metropolitan region. Tokyo Bay, large-scale industries, and residential areas are located within a 50 km radius. The Chiba site is also affected by ship emissions from Tokyo Bay. The Chiba climate is the following: (1) spring (March–May), (2) summer (June–August), (3) autumn (September–November), and winter (December– February). The locations of the three sites are portrayed in Fig. 1.

https://doi.org/10.5194/acp-2021-815
Preprint. Discussion started: 25 October 2021

Atmospheric Chemistry and Physics Discussions

128

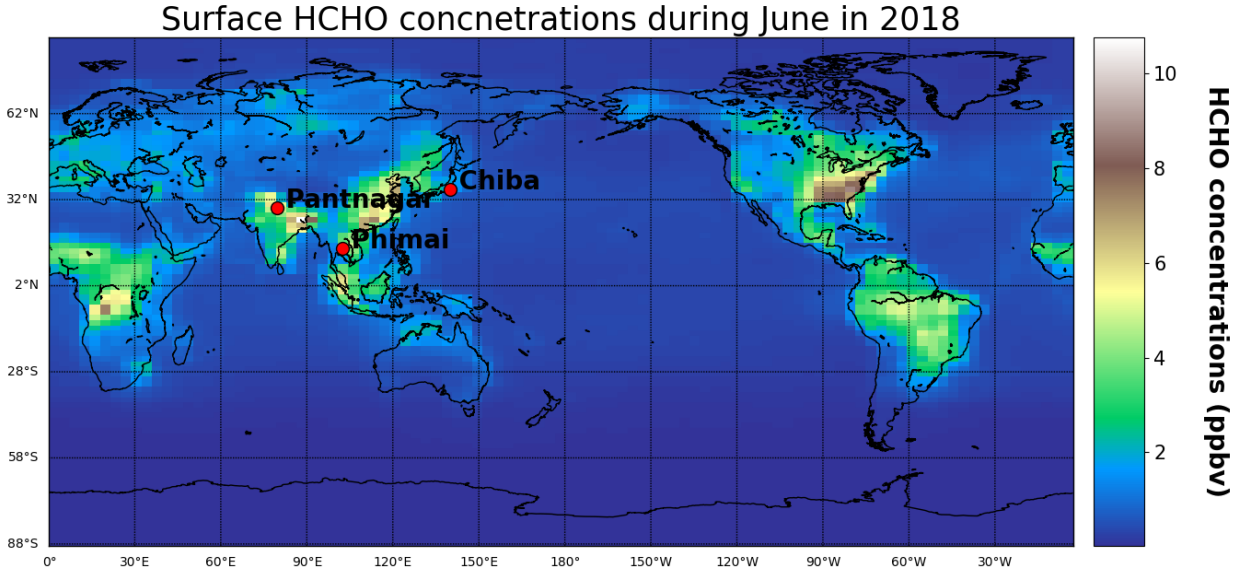

129 **Figure 1:** Surface HCHO concentrations during June 2018, simulated using the CHASER model. The
130 red points indicate the locations of the observation sites, which are part of the A-SKY network.

131

132

133

134

135 ## 2.2 MAX-DOAS retrieval

136

137 The MAX-DOAS systems used for continuous observations at the three sites participated in the Cabauw
138 Intercomparison Campaign of Nitrogen Dioxide measuring Instruments (CINDI) (Roscoe et al., 2010)
139 and CINDI-2 (Kreher et al., 2020) campaign. The instrumentation setup was described by Irie et al. (2008,
140 2011, 2015). The indoor part of the MAX-DOAS systems consisted of an ultraviolet-visible (UV-VIS)

https://doi.org/10.5194/acp-2021-815
Preprint. Discussion started: 25 October 2021


Atmospheric Chemistry and Physics Discussions

spectrometer (Maya2000Pro; Ocean Optics Inc.) embedded in a temperature-controlled box. A telescope unit was situated outdoors. The outdoor unit was a single telescope and a 45° inclined movable mirror on a rotary actuator, used to perform reference and off-axis measurements. The high-resolution spectra from 310–515 nm were recorded at six elevation angles (ELs) of 2°, 3°, 4°, 6°, 8°, and 70° at the Chiba and Phimai sites. At the Pantnagar site, measurements were conducted at ELs of 3°, 4°, 5°, 6°, 8°, and 70°. The sequences of the ELs at all the sites were repeated every 15 min. The reference spectra were recorded at EL of 70° instead of 90° to minimize variations in the signals measured at each EL. The off-axis ELs were limited to < 10° to reduce the systematic error in the in-oxygen collision complex (O_4) fitting results (Irie et al., 2015), thereby maintaining high sensitivity in the lowest layer of the retrived aerosol and trace gas profiles. Daily wavelength calibration using the high-resolution solar spectrum from Kurucz et al. (1984) was performed to account for the spectrometer's probable long-term degradation. The spectral resolution (full width half maximum: FWHM) was about 0.4 nm at 357 and 476 nm. The concentrations and profiles of aerosol and trace gases were retrieved using the Japanese vertical profile retrieval algorithm (JM2 ver. 2) (Irie et al., 2011, 2015). The algorithm works in three steps: (1) DOAS fittings, (2) profile/column retrieval of aerosol, and (3) profile/column retrieval of trace gases. Irie et al. (2008a, 2008b, 2011, 2015) described the retrieval procedures and the error estimates. Here we provide a short overview.

First, the differential slant column density (ΔSCD) of trace gases was retrieved using the DOAS technique (Platt 1994), which uses the nonlinear least-squares spectral fitting method, according to the following equation.

$$lnI(\lambda) = ln(I_o(\lambda) - c(\lambda)) - \sum_{i}^{n} \sigma_i(\lambda)\Delta SCD_i - p(\lambda) \quad (1)$$

Therein, $I_o(\lambda)$ represents the reference spectrum measured at time *t*. Actually, $I_o(\lambda)$ was derived by interpolating two reference spectra (i.e., EL=70°) within 15 min before and after the complete sequential scan of the off-axis ELs at time *t*. ΔSCD represents the difference between the slant column density along the off-axis and reference spectrum. Second-order and third-order polynomials were fitted to account for

https://doi.org/10.5194/acp-2021-815
Preprint. Discussion started: 25 October 2021

Atmospheric Chemistry and Physics Discussions

the wavelength-dependent offset $c(\lambda)$ and the effect because of molecular and particle scattering $p(\lambda)$, respectively. Also, $c(\lambda)$ accounts for the influence of stray light. The HCHO ΔSCD and NO_2 ΔSCD are retrieved respectively from the fitting windows of 336–359 nm and 460–490 nm. The O_4 ΔSCD values were retrieved from the fitting windows of 338–370 and 460–490 nm, where significant O_4 absorptions occur. The absorption cross-section data used and the absorbers fitted in the HCHO and NO_2 fitting windows are similar to those of Hoque et al. (2018a, 2018b). Figure 2 presents an example of the fitting results.

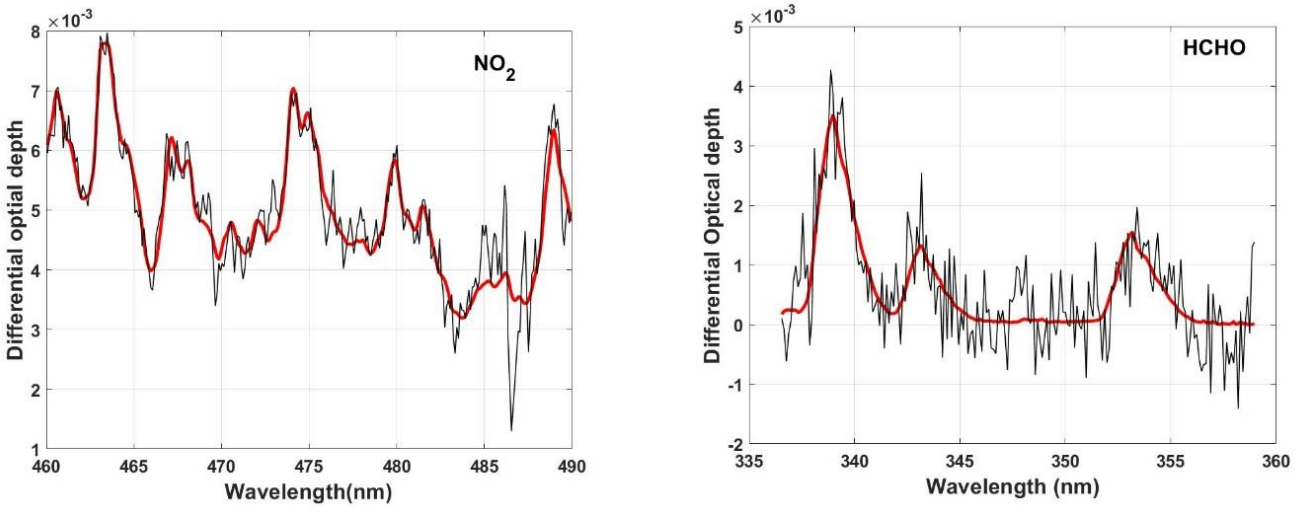

Figure 2: Examples of spectral fitting of NO_2 and HCHO, where the red and black lines show the DOAS fittings and summation of scaled cross-sections and fitting residuals, respectively. The example is shown for the measurements on 10 April 2017, in Phimai at 10:00 LT at an EL of 2°.

https://doi.org/10.5194/acp-2021-815
Preprint. Discussion started: 25 October 2021


Atmospheric Chemistry and Physics Discussions

In the second step, the aerosol optical depth (AOD) τ and the vertical profiles of the aerosol extinction coefficient (AEC) k were retrieved using the optimal estimation method (Irie et al., 2008a; Rogers, 2000) The measurement vector y (representing the quantities to be fitted) and state vector (representing the retrieved quantities) are defined as

$$y = (O_4 \Delta SCD(\Omega_1) \dots \dots \dots \Delta SCD(\Omega_n))^T \quad (2) \text{ and}$$

$$x = (\tau F_1 F_2 F_3)^T \quad (3),$$

where n stands for the number of measurements within one complete scan of an EL sequence. Also, Ω denotes the viewing geometry, comprising three components: solar zenith angle (SZA), EL, and relative azimuth angle (RAA). The F values determine the profile shape, with values between 0 and 1. The partial AOD for 0–1, 1–2, 2–3, and above 3 km layers were defined respectively as AOD ·F_1, AOD ·(1-F_1) F_2, and AOD · (1-F_1) (1-F_2) F_3, and AOD ·(1-F_1) (1-F_2) (1-F_3). The AEC profile from layer 3 to 100 km was derived assuming a fixed value at 100 km and exponential AEC profile shape. Similarly, the AEC profiles at 2–3, 1–2, and 0–1 km were derived. Such parameterization provides the advantage that the AEC profile can be retrieved with only the apriori knowledge of the F (profile shape) values and little or no information related to the absolute AEC values in the troposphere. Irie et al. (2008a) demonstrated that the relative variability of the profile shape, in terms of 1-km averages, is smaller than that of the absolute AEC values. However, the vertical resolution and the measurement sensitivity cannot be derived instantly with such parameterization (Irie et al., 2008a; 2009). To overcome such limitations, the retrievals and simulations conducted by other groups for similar geometry (i.e., Frieß et al., 2006) were used. The apriori values used for this study were similar to those reported by Irie et al. (2011): AOD = 0.21 ± 3.0, F_1 = 0.60 ± 0.05, F_2 = 0.80 ± 0.03, and F_3 = 0.80 ± 0.03.

Then, a lookup table (LUT) of the box air mass factor (A_{box}) vertical profile was constructed using the radiative transfer model JACOSPAR (Irie et al., 2015), which is based on the Monte Carlo Atmospheric Radiative Transfer Simulator (MCARaTS) (Iwabuchi, 2006). Results obtained from JACOSPAR were

https://doi.org/10.5194/acp-2021-815
Preprint. Discussion started: 25 October 2021


Atmospheric Chemistry and Physics Discussions

validated in the study of Wagner et al. (2007). The optimal aerosol loading and the A_{box} profiles were derived using the A_{box} LUT and the O_4 ΔSCD at all ELs.

In the third step, the A_{box} profiles, HCHO ΔSCD and NO_2 ΔSCD, and the nonlinear iterative inversion method were used to retrieve the HCHO and NO_2 vertical column densities (VCDs) and profiles. Here the NO_2 retrieval is explained.

For trace gas retrieval, the measurement vector and state vector were defined as

$$y = (NO2\Delta SCD(\Omega_1) \dots \dots \dots NO2\Delta SCD(\Omega_n))^T \quad (4)$$ and

$$x = (VCD f_1 f_2 f_3)^T \quad (5)$$

In those equations, VCD represents the vertical column below 5 km; f values are the profile shape factor. Above the 5 km layer, fixed profiles are assumed. Similarly, to aerosol retrieval, the partial VCD for the 0–1, 1–2, 2–3, and 3–5 km was defined respectively as VCD ·f_1, VCD ·(1-f_1) f_2, VCD · (1-f_1) (1-f_2) f_3, and VCD ·(1-f_1) (1-f_2) (1-f_3). The partial VCD values are converted to the volume mixing ratio (VMR) using the U.S. standard atmosphere temperature, and pressure data scaled to the respective site surface measurements.

The calculated vertical profile was converted to NO_2 ΔSCD using the A_{box} LUT constructed for aerosol retrieval. However, the trace gas wavelengths differed from the representative wavelengths of A_{box} LUT (357 and 476 nm). The AOD at the trace gas wavelength was estimated, converting the retrieved AOD to the closer aerosol wavelength of 357 or 476 nm, assuming the Angstrom exponent value as 1.00. Then, the A_{box} profiles from the LUT corresponding to the recalculated AOD values were selected. Dependence of the A_{box} profiles on the concentration profiles is expected to be minimal because both HCHO and NO_2 are optically thin absorbers. (Wagner et al., 2007; Irie et al., 2011). For every 15 min (time required for one complete scan of ELs, 20%, the mean ratio of retrieved VCD to maximum ΔSCD) of the maximum trace gas ΔSCD was used as a priori information for VCD retrieval. The a priori error was set to 100% of the maximum trace gas ΔSCD. Figure 3 presents the mean averaging kernel of the HCHO and NO_2 retrievals during the dry season in Phimai. The area calculated from the averaging kernel was close to unity. Therefore, the retrieved VCD was independent of the a priori values.

https://doi.org/10.5194/acp-2021-815
Preprint. Discussion started: 25 October 2021

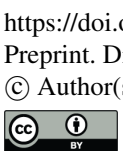

Atmospheric Chemistry and Physics Discussions

235

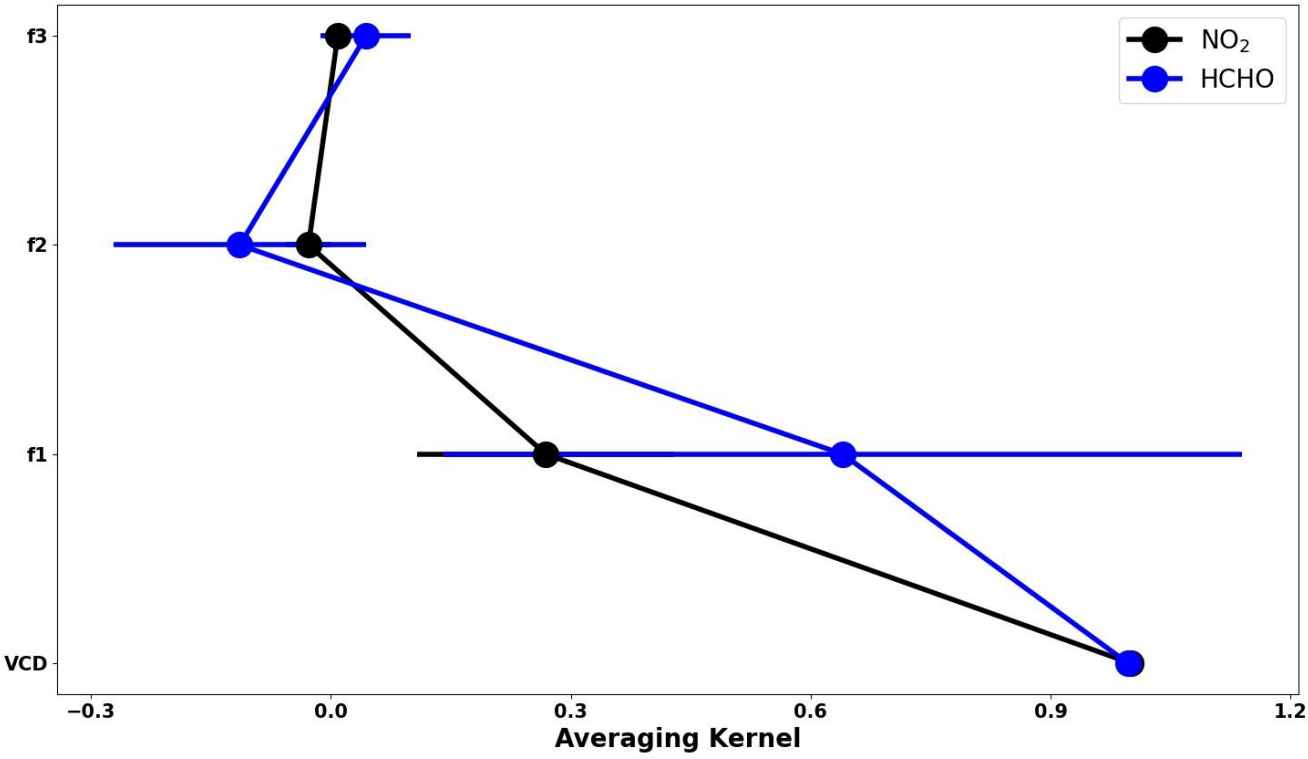

236

237 **Figure 3:** The mean averaging kernel of the NO_2 and HCHO retrievals from the observations in Phimai during
238 2017

239

240 The total error of the retrieval consists of random and systematic errors. The measurement error
241 covariance matrix constructed from the residuals of the respective trace gas ΔSCDs was used to estimate
242 the random error. The systematic error was calculated assuming uncertainties as high as 30 and 50% in
243 the retrieved AOD (or the corresponding A_{box} values). The estimated total error is shown in Table 1. Aside
244 from the random and systematic error, more sources of error might exist. For instance, the bias in the ELs
245 can induce uncertainties in the retrieved products. However, Hoque et al. (2018) demonstrated that such
246 biases had a non-significant effect on the final retrieved products, mostly less than 5%.

247 The cloud screening procedure was similar to that described by Irie et al. (2011) and by Hoque et al.
248 (2018a, 2018b). During the retrieval steps, retrieved AOD values > 3 were excluded. Optically thick

https://doi.org/10.5194/acp-2021-815
Preprint. Discussion started: 25 October 2021

Atmospheric Chemistry and Physics Discussions

clouds are primarily responsible for such large optical depth. Furthermore, cloud influence was filtered based on the residuals of O_4 and the trace gas ΔSCDs. The screening criteria were: respective residuals of O_4, HCHO, and NO_2 of ΔSCD < 10%, < 50%, and <20%, and the degrees of freedom of the retrieval greater than 1.02.

Table 1. Estimated Errors (%) for the NO_2 and HCHO concentration in 0-1 km layer, retrieved using theJM2 algorithm

Retrieved Product	Random error	Systematic error	Error related to instrumentation	Total error
NO_2	10	12	5	16
HCHO	16	25	5	30

2.3 CHASER simulations

CHASER V4.0 (Sudo et al., 2002; Sudo and Akimoto, 2007; Sekiya and Sudo, 2014), coupled online with the MIROC-AGCM atmospheric general circulation model (AGCM) (K-1 model developers, 2004) and the SPRINTARS aerosol transport model (Takemura et al., 2005, 2009), is a global chemistry transport model to study the atmospheric environment and radiative forcing. In addition, several updates, including the introduction of aerosol species (sulfate, nitrate, etc.) and related chemistry, radiation, and cloud processes, have been implemented in the latest version of CHASER.

CHASER can calculate the concentrations of 92 species through 263 chemical reactions (gaseous, aqueous, and heterogeneous chemical reactions) considering the chemical cycle of O_3–HO_x – NO_x –CH_4–CO along with oxidation of non-methane volatile organic compounds (NMVOCs)(Miyazaki et al., 2017). CHASER simulates the stratospheric ozone chemistry considering the Chapman mechanisms, catalytic reactions related to halogen oxides (HO_x, NO_x, ClO_x, and BrO_x), and polar stratospheric clouds (PSCs). Resistance-based parameterization (Wesely, 1989), cumulus convection, and large-scale condensation

https://doi.org/10.5194/acp-2021-815
Preprint. Discussion started: 25 October 2021


Atmospheric Chemistry and Physics Discussions

parameterizations are used to calculate dry and wet depositions. The piecewise parabolic method (Colella and Woodward, 1984) scheme and the flux-form semi-Lagrangian scheme (Lin and Rood, 1996) calculate the advective tracer transport. CHASER simulates tracer transport on a sub-grid scale in the framework of the prognostic Arakawa–Schubert cumulus convection scheme (Emori et al., 2001) and the vertical diffusion scheme (Mellor and Yamada, 1974). In this study, CHASER simulations were conducted at a horizontal resolution of 2.8° × 2.8°, with 36 vertical layers from the surface to ~50 km altitude and a typical time step of 20 min. The meteorological fields simulated by MIROC-AGCM were nudged toward the six-hourly NCEP FNL reanalysis data at every model time step.

The anthropogenic, biomass burning, lightning, and soil emission sources of NO_x were incorporated into CHASER simulations. Anthropogenic emissions were based on the HTAP_v2.2 for 2008. Emissions from biomass burning and soils were inferred based on the ECMWF/MAC reanalysis. The biogenic emissions for VOCs are based on the process-based biogeochemical model the Vegetation Integrative SImulator for Trace gases (VISIT) (Ito and Inatomi, 2012). The NO_x production from lightning is calculated based on the parameterization presented by Price and Rind (1992) linked to the convection scheme of the AGCM (Sudo et al., 2002). The isoprene, terpene, acetone, and ONMV emissions during July were, respectively, 2.14×10^{-11}, 4.43×10^{-12}, 1.60×10^{-12}, and 9.93×10^{-13} $kgCm^{-2}s^{-1}$.

Multiple CHASER simulations with different settings used for this study are presented in Table 2.

https://doi.org/10.5194/acp-2021-815
Preprint. Discussion started: 25 October 2021


Atmospheric Chemistry and Physics Discussions

300 **Table 2 :** The settings of the CHASER simulations used in the current study

Simulation	Anthropogenic emissions	Pyrogenic emissions	Biogenic emissions	Other physical and chemical processes
Standard	ON	ON	ON	ON
L1_HCHO	ON	Pyrogenic VOCs switched OFF	ON	ON
L1_opt	ON	Pyrogenic VOCs switched OFF	Reduced by 50%	ON
L1_NO_2	ON	Pyrogenic NO_2 emissions switched OFF	ON	ON
L2	Anthropogenic VOC emissions switched OFF	ON	ON	ON

301
302
303
304
305

https://doi.org/10.5194/acp-2021-815
Preprint. Discussion started: 25 October 2021

3 Results and discussion

3.1 Results from MAX-DOAS observations

3.1.1 HCHO seasonal variation

The monthly mean HCHO concentrations in the 0–1 and 0–2 km layers from January 2017 – December 2018 and the corresponding one sigma (1σ) standard deviations for the three sites are depicted in Fig. 4. The HCHO amounts at the Phimai site present a consistent seasonal cycle, characterized by high concentrations during the dry season. Such enhancement is related to the influence of biomass burning during the dry season, which has been well documented in the work of Hoque et al. (2018). The HCHO concentrations at Phimai peak in March or April, and the maximum concentrations of 4–6 ppbv. The variation in the peak concentration and timing mainly depend on the intensity of biomass burning activities. During the wet season, the HCHO concentrations are primarily within 2–3 ppbv, indicating a two-fold increase in the HCHO abundances during the dry season. The daily mean HCHO amounts (0–1 km) are 9.84–0.78 ppbv, representing seasonal modulation of 134%.

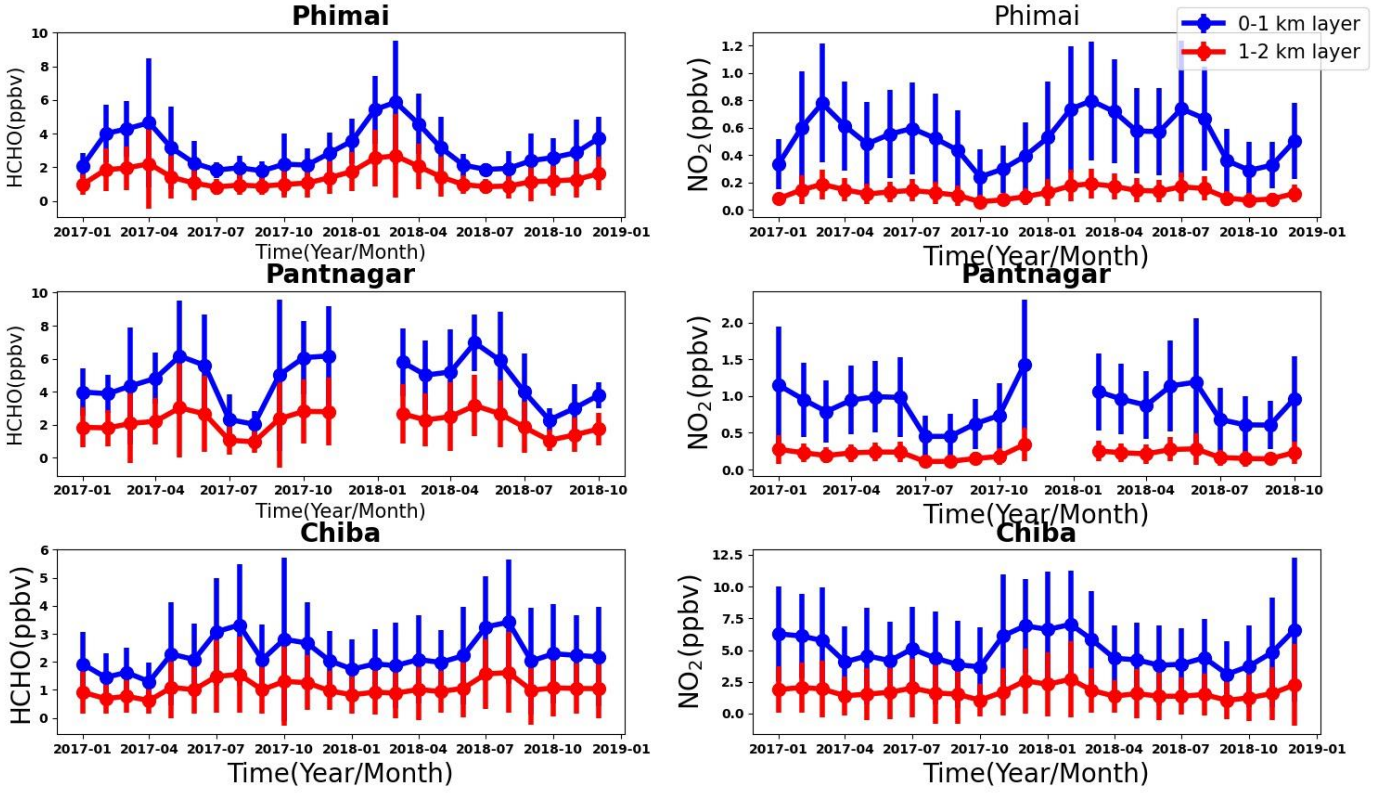

https://doi.org/10.5194/acp-2021-815
Preprint. Discussion started: 25 October 2021


Atmospheric Chemistry and Physics Discussions

319

320 **Figure 4:** The seasonal variations in the HCHO (left panel) and NO_2 (right panel) concentrations in the 0-1 (blue)
321 and 1-2 (red) km layers in Phimai, Pantnagar, and Chiba. The error bars indicate the one sigma standard deviation
322 of the mean values. The gaps in the plots for the Pantnagar site indicate the unavailability of observations during
323 the investigated period.

324

325

326 The seasonal variation of HCHO in the 0–1 km layer at the Pantnagar site has been discussed by
327 Hoque et al. (2018b). Here, the results are replotted to verify the consistency of the seasonal variations.
328 Observations made during autumn in 2018 were not available because of technical glitches in the
329 spectrometer. Consistent seasonal variation of HCHO abundances is observed at the Pantnagar site, with
330 enhanced concentrations during the spring. The Pantnagar site is affected by biomass burning during
331 spring and autumn (Hoque et al., 2018b), explaining the high concentrations found during spring. In both
332 years, the maximum HCHO concentrations were ~6 ppbv. The springtime peak occurred in May. The
333 HCHO concentrations during the monsoon are ~35% lower than in the spring, indicating a strong effect
334 of the monsoon on the HCHO concentrations found for Pantnagar. The seasonal modulation of HCHO at
335 Pantnagar estimated from the daily mean concentrations is 107%. Under the influence of biomass burning,
336 the maximum monthly HCHO concentrations are similar (~6 ppbv) at Phimai and Pantnagar. The
337 maximum instantaneous concentrations of HCHO during biomass burning influence in Phimai and
338 Pantnagar are 26 and 30 ppbv, respectively. Zarzana et al., (2017) reported HCHO abundances of ~60
339 ppbv in fresh biomass plumes in the US. The lower values obtained from our measurements might be
340 attributable to (1) more aged plumes intercepted by the MAX-DOAS instruments and (2) differences in
341 the types of biomass fuel used. However, comparison of the literature values indicates that our retrieval
342 values of HCHO under biomass burning are reasonable.

343 Higher concentrations characterize the seasonal variation of HCHO at the Chiba site during summer,
344 with a peak ~3 ppbv, likely produced from the oxidation of biogenic VOCs, from which emissions
345 increase with the rising ambient temperature. The HCHO concentrations are ~2 ppbv during another
346 seasons, similar to the HCHO concentrations in Phimai during the wet season. The seasonal modulation

https://doi.org/10.5194/acp-2021-815
Preprint. Discussion started: 25 October 2021


Atmospheric Chemistry and Physics Discussions

of HCHO in Chiba was ~94%. For a site with similar seasonal variation (i.e., summertime maximum and wintertime minimum), Franco et al. (2015) reported seasonal modulation of HCHO as ~. 88%.

The concentrations of HCHO in the 1–2 km layers at all three sites were lower, almost 50% the value of the concentrations in the 0–1 km layer. The HCHO seasonal modulations at Phimai, Pantnagar, and Chiba sites were, respectively, 131%, 102%, and 90% when calculated based on the HCHO concentration in the 1–2 km layers. The modulation further decreased when retrieved values for 2–3 km layer were used. This finding highlights the strong sensitivity of the MAX-DOAS instrument for near-surface layers, mainly within the planetary boundary layer.

3.1.2 NO_2 seasonal variation at the three sites

Figure 4 also shows the seasonal variation of NO_2 for 0–1 and 1–2 km layers at the three sites. The error bar represents 1σ standard deviation of the mean values. The NO_2 seasonal variations at Phimai and Pantnagar sites are similar to those of HCHO. A pronounced peak attributable to biomass burning influence is observed during the dry season in Phimai (~0.8 ppbv) and the spring (1.2 ppbv), and the post-monsoon period (1.4 ppbv) in Pantnagar. The lowest NO_2 concentrations in Phimai and Pantnagar were, respectively, ~0.2 and 0.5 ppbv. The NO_2 concentration in Chiba was higher (~7 ppbv) during winter. The longer lifetime of NO_x and lower NO/NO_2 ratio because of lower photochemical activity in winter engender high NO_2 concentrations in Chiba (Irie et al., 2021).

At Phimai, high NO_2 concentrations are observed during the wet season. When Hoque et al. (2018) reported the seasonal variation of NO_2 at Phimai during 2015–2016, such high NO_2 concentrations in the wet season were not observed. It is unlikely that such high concentrations are related to biomass burning. Otherwise, a similar peak would have appeared in the HCHO seasonal variation during the wet season. We also checked the concentrations of glyoxal (CHOCHO) and O_3 (Fig. S1, supplement information) for additional confirmation, simultaneously retrieved using JM2. No enhancement was observed during the wet season. A potential source of NO_2 concentrations during the wet season is NO_x emissions from soil. Although NO_2 is not emitted directly from soils, biological processes in the soil emit NO, which is rapidly converted to NO_2 (Hall et al., 1996). Many studies have established a relation between soil moisture and NO emissions (Carden et al., 1993; Zheng et al., 2000; Schindlbacher et al., 2004; Huber et al., 2020). We use soil moisture data from Soil Moisture Active Passive (SMAP) satellite data to infer the potential

https://doi.org/10.5194/acp-2021-815
Preprint. Discussion started: 25 October 2021


Atmospheric Chemistry and Physics Discussions

375 contribution of soil NO_x emissions to NO_2 concentrations in Phimai during the wet season. Daily
376 composite soil moisture data (Level 3) with horizontal resolution of 36 km are used for analysis. The data
377 were screened based on the retrieval quality flag, as explained in the user guide document
378 (https://nsidc.org/data/SPL3SMP/versions/7, last accessed on 18/05/2021). SMAP observations within
379 the 30 km radius of the Phimai site were selected. Details of the SMAP datasets have been described by
380 Colliander et al. (2017).

381 Figure 5 shows the monthly and daily MAX-DOAS NO_2 concentrations for the 0–1 km layer in
382 Phimai and the SMAP soil moisture and surface temperature data. The coincident dates between the
383 MAX-DOAS and SMAP observations are shown. The expected increase in the soil moisture during the
384 wet season coincided with the high NO_2 concentration in the wet season, indicating more substantial soil
385 NO_x emissions than the dry season. Actually, NO_2 concentrations greater than 0.6 ppbv are primarily
386 associated with soil moisture >40%. Few inconsistencies are observed where the NO_2 concentrations and
387 soil moisture show a reciprocal relation. Reports of many studies have described a negative relation
388 between NO_x emissions and soil moisture (Levine et al., 1990; Davidson et al., 1991; Yamulki et al.,
389 1995). In general, NO_x emissions are more potent at intermediate moisture levels and are comparatively
390 low when the soil is dry or saturated because the additional water fills the pore spaces and restricts NO_x
391 diffusion (Hall et al., 1996). This explanation is consistent with the lower NO_2 concentrations at the end
392 of the wet season despite the higher soil moisture. In addition to soil moisture, the surface temperature is
393 a governing factor for soil NO_x emissions. However, in Phimai, the temperature variation is ~2 K during
394 the wet season, indicating a less significant role in soil NO_x emissions than soil moisture.

395 Because NO_2 emissions from soils are included in CHASER simulations, we attempted to quantify
396 the NO_2 contributions from soil emissions. Figure 5d presents the monthly mean surface NO_2
397 concentrations in Phimai in 2017, simulated including and switching off the soil NOx emissions. The
398 NO_2 concentrations between 09 and 12 hr were used to calculate the monthly mean concentrations. Soil
399 emissions contribute ~20% of the overall NO_2 concentrations in Phimai, with higher contributions during
400 the wet season. The peak NO_2 concentration (Fig. 3a)) and high soil moisture (Fig. 3b) in July 2017
401 coincide with CHASER sensitivity results, showing the highest contributions (~25%) from soils

https://doi.org/10.5194/acp-2021-815
Preprint. Discussion started: 25 October 2021

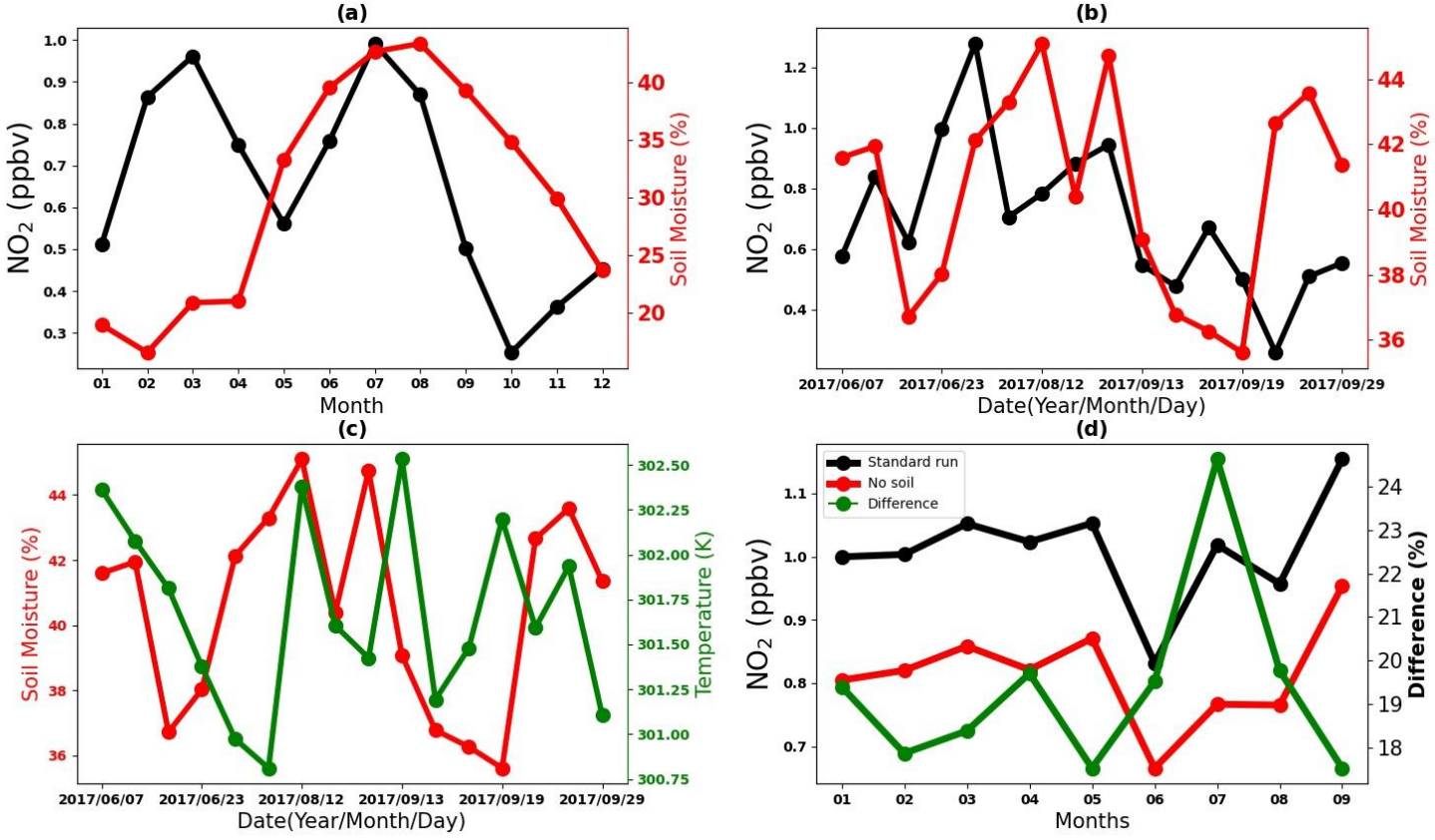

Figure 5. (top panel) (a) The seasonal variation of NO_2 concentrations (black colour) in the 0- 1 km layer and the soil moisture (red colour), retrieved from the MAX-DOAS and SMAP observations, respectively, in Phimai. The coincident days between the MAX-DOAS and SMAP observations were selected to calculate the seasonal mean values. (b) The daily mean NO_2 concentrations (black colour) in the 0-1 km layer and the soil moisture (red colour) are plotted for the wet season's coincident dates. (bottom panel) (c) The surface temperature (green colour) and soil moisture during the wet season, retrieved from SMAP observations, are plotted. Both parameters are plotted on the dates when MAX-DOAS observations are available. (d) CHASER simulated NO_2 concentrations in Phimai, including (black)and switching off (red) the soil NOx emissions. The green line indicates the percentage difference between the two simulations.

https://doi.org/10.5194/acp-2021-815
Preprint. Discussion started: 25 October 2021


Atmospheric Chemistry and Physics Discussions

415

416 occur during July. Consequently, high NO_2 concentrations found during the wet season can be attributed
417 to soil NO_x emissions.

418 The question arises of why such features (high NO_2 concentrations during the wet season) were not
419 found in an earlier study (i.e., Hoque et al., 2018a). The change in soil moisture might explain such a
420 discrepancy. According to our observations, the soil moisture in Phimai is governed by the amount of
421 rainfall. To verify the consistency of the rainfall amounts in Phimai during the wet season, coincident
422 microwave radiometer observations made in 2016 and 2018 were used (Fig. S2, in the supplement
423 information). No significant difference in the precipitable water content was found for those years, which
424 indicates that soil moisture tends to be a less important factor underlying the discrepancy. No discrepancy
425 among our studies is apparent. Our future studies will include detailed discussion of this issue.

426

427 **3.1.3 The HCHO to NO_2 ratio (R_{FN}):**

428 The HCHO to NO_2 (R_{FN}) ratio is regarded as an indicator of O_3 sensitivity (Martin et al., 2004; Duncan
429 et al., 2010). In this section, the R_{FN} values found for the sites are discussed. To estimate the R_{FN} values,
430 we use the HCHO and NO_2 concentrations in the 0–1 km layer. For discussion of the R_{FN} values, we also
431 used the O_3 concentrations for the 0–1 km layer retrieved from our MAX-DOAS observations. Details of
432 the O_3 retrieval procedure in the JM2 algorithm are explained by Irie et al. (2011). For minimization of
433 stratosphere effects, we used only the O_3 concentrations for SZA < 50°. Irie et al. (2021) reported good
434 agreement between the O_3 concentrations retrieved using JM2 and ozonesonde measurements.

435 Figure 6 shows a scatter plot of daily mean NO_2 and HCHO concentrations, color-coded with the
436 respective O_3 concentrations measured at the respective sites. The O_3 production regime is regarded as
437 VOC-limited for $R_{FN} < 1$ and NO_x limited to when $R_{FN} > 2$ (Duncan et al., 2010; Ryan et al., 2020). This
438 assumption of the R_{FN} values is valid for HCHO concentrations < 10 ppbv (Souri et al., 2020).
439 Consequently, R_{FN} values for HCHO concentrations < 10 ppbv are shown. Almost all high O_3
440 concentrations (>40 ppbv) coincide with the $R_{FN} > 2$ regimes at Phimai and Pantnagar. Only a few, if any,
441 cases were in the $R_{FN} < 1$ regime. At Phimai, few instances during the wet season ($O_3 < 20$ ppbv) lay in
442 the transition region ($1 < R_{FN} < 2$). Results show that the O_3 production regime is NO_x limited at both sites.

https://doi.org/10.5194/acp-2021-815
Preprint. Discussion started: 25 October 2021

Atmospheric Chemistry and Physics Discussions

443 At Chiba, most high O_3 concentration (>80 ppbv) cases are related to high NO_2 concentrations, indicating
444 a VOC-limited regime, which is consistent with results reported by Irie et al. (2021).
445
446

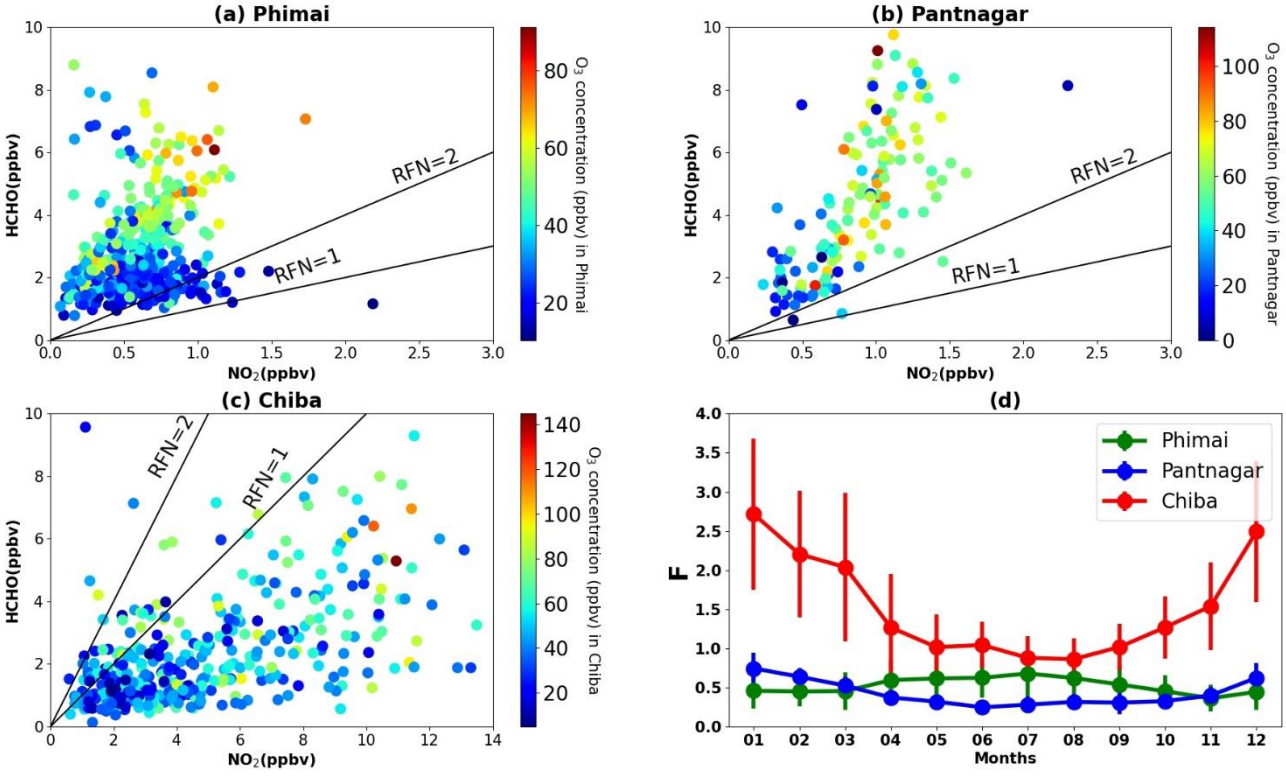

447 **Figure 6.** The scatter plot of HCHO and NO_2 concentrations in the 0-1 km layer at (a) Phimai, (b) Pantnagar, and
448 (c) Chiba, coloured with the O_3 concentrations in the 0-1 km layer at the respective sites. The solid lines indicate
449 R_{FN} = 2 and R_{FN} =1 benchmark. (d) The seasonal variations in the column to surface conversion factor (F) for the
450 Phimai, Pantnagar, and Chiba sites, estimated from the CHASER simulated HCHO and NO_2 surface concentrations
451 and vertical column density. The simulated data from 07:00 – 18:00 in 2017 were used to estimate the F values.
452 The error bars indicate the one sigma standard deviation of the mean values.
453

454 Mahajan et al. (2015) reported OMI-derived R_{FN} values < 1 over the IGP region, which contradicts
455 our findings for Pantnagar. However, the R_{FN} values at Pantnagar are consistent with the values reported
456 by Biswas et al. (2019), derived from MAX-DOAS observation at another site in the IGP region. The O_3

https://doi.org/10.5194/acp-2021-815
Preprint. Discussion started: 25 October 2021


Atmospheric Chemistry and Physics Discussions

457 sensitivity inferred from the R_{FN} values estimated from satellite and surface in-situ measurements showed
458 different results because of the gradient of the R_{FN} values. Jin et al. (2017) proposed the idea of a
459 conversion factor to account for gradient differences in the surface and column-derived R_{FN} values,
460 estimating the conversion factor from the model simulated surface and column abundances of NO_2 and
461 HCHO. For this study, we adopt the method reported by Jin et al. (2017) using the CHASER simulated
462 NO_2 and HCHO concentrations and vertical columns.

463 First, the CHASER simulated near-surface NO_2 and HCHO concentrations were converted to number
464 density and the effective boundary layer height (E) (Halla et al., 2011; Jin et al., 2017) was estimated.

465

466 $$E_{NO_2} = \frac{NO_2\ total\ coulmn}{NO_2\ near-surface\ number\ density} \quad (6)$$

467

468 $$E_{HCHO} = \frac{HCHO\ total\ coulmn}{HCHO\ near-surface\ number\ density} \quad (7)$$

469 Therein, E_{NO_2} and E_{HCHO} respectively denote the effective boundary layer heights of NO_2 and HCHO.
470 In the second step, the column to surface conversion factor (F) was calculated according to the following
471 equation:

472 $$F = \frac{E_{HCHO}}{E_{NO_2}} \quad (8)$$

473 The seasonal variation of F for the three A-SKY sites and the associated 1σ standard deviation of the
474 mean values are depicted in Fig. 6d. The F values over East Asia reported by Jin et al. (2017) were ~2,
475 with no marked seasonal variation. Compared to values reported in the literature, the CHASER estimated
476 F values over Chiba range between 1–2.5, which seems reasonable. The reason for the discrepancy in the
477 F values can be (1) the difference in the model resolutions between the literature and current study, (2)
478 the literature values are reported for polluted regions (NO_2 > 2.5 molecules cm^{-2}) and considered the
479 simulation data for 1–2 PM. By contrast, the estimates of this study included daytime (07:00 – 18:00)
480 values.

https://doi.org/10.5194/acp-2021-815
Preprint. Discussion started: 25 October 2021


Atmospheric Chemistry and Physics Discussions

The F values in Pantnagar are mostly < 1, with no distinctive seasonal variation. When this estimated conversion factor is used with the values of Mahajan et al. (2015) (i.e., OMI derived R_{FN} values < 1 over the IGP region), the discrepancy in the satellite and ground-based observation derived R_{FN} values in the IGP region are reduced, indicating that the estimated F values for the Pantnagar site can be representative for the IGP region. The F values at the Phimai site range were 0.5–1. No report of the relevant literature presents F values for the southern and southeastern Asian regions. Consequently, our estimated *F* values for the Phimai and Pantnagar site are useful as representative values for these respective regions, which can be improved further based on the results.

3.1.4 Can the glyoxal to formaldehyde (R_{GF}) ratio be used as an indicator of ozone sensitivity?

Ryan et al. (2020) proposed that, in addition to the R_{FN}, the glyoxal to formaldehyde ratio (R_{GF}) can also be a helpful indicator of O_3 production regimes and concentrations because VOCs are an important component in the VOC- HO_x-NO_x catalytical cycle governing O_3 production. We use the coincident glyoxal (CHOCHO) concentrations retrieved using the JM2 algorithm and the O_3 concentrations to test this hypothesis. Detailed procedures and error estimates of the CHOCHO retrievals are explained by Irie et al. (2011) and by Hoque et al. (2018a). The R_{GF} values estimated from HCHO and CHOCHO retrieved using the JM2 algorithm have been discussed by Hoque et al. (2018a, 2018b). Figure 7 shows a scatter plot of the daily mean CHOCHO and HCHO concentrations, colored with the O_3 concentrations for the three sites. The R_{GF} values are < 0.04 when VOC sources are dominantly anthropogenic or pyrogenic, whereas higher R_{GF} values are observed under the dominant biogenic sources of VOCs (Hoque et al., 2018a; Vrekoussis et al., 2009). At the three sites, high O_3 concentrations (>40 ppbv) are associated primarily with R_{GF} < 0.04, consistent with findings reported by Ryan et al. (2020). However, for O_3 concentrations below 20 ppbv, the robustness of the R_{GF} decreases. At all three sites, many cases are found when the lower O_3 concentrations are associated with R_{GF} values less than 0.04. Moreover, two issues should be accounted for before using R_{GF} as an indicator of O_3 production sensitivity. (1) The change of R_{GF} under different VOC emission scenarios is still under discussion. There are contrasting results from field observations (Digangi et al., 2012; Kaiser et al., 2015; etc.). (2) Also, the gradient of the R_{GF} values is not well understood because few studies have particularly addressed the issue. Therefore,

https://doi.org/10.5194/acp-2021-815
Preprint. Discussion started: 25 October 2021

509 we infer that a more detailed analysis is necessary to regard R_{GF} as an indicator of O_3 sensitivity, in
510 addition to R_{FN}.
511
512
513

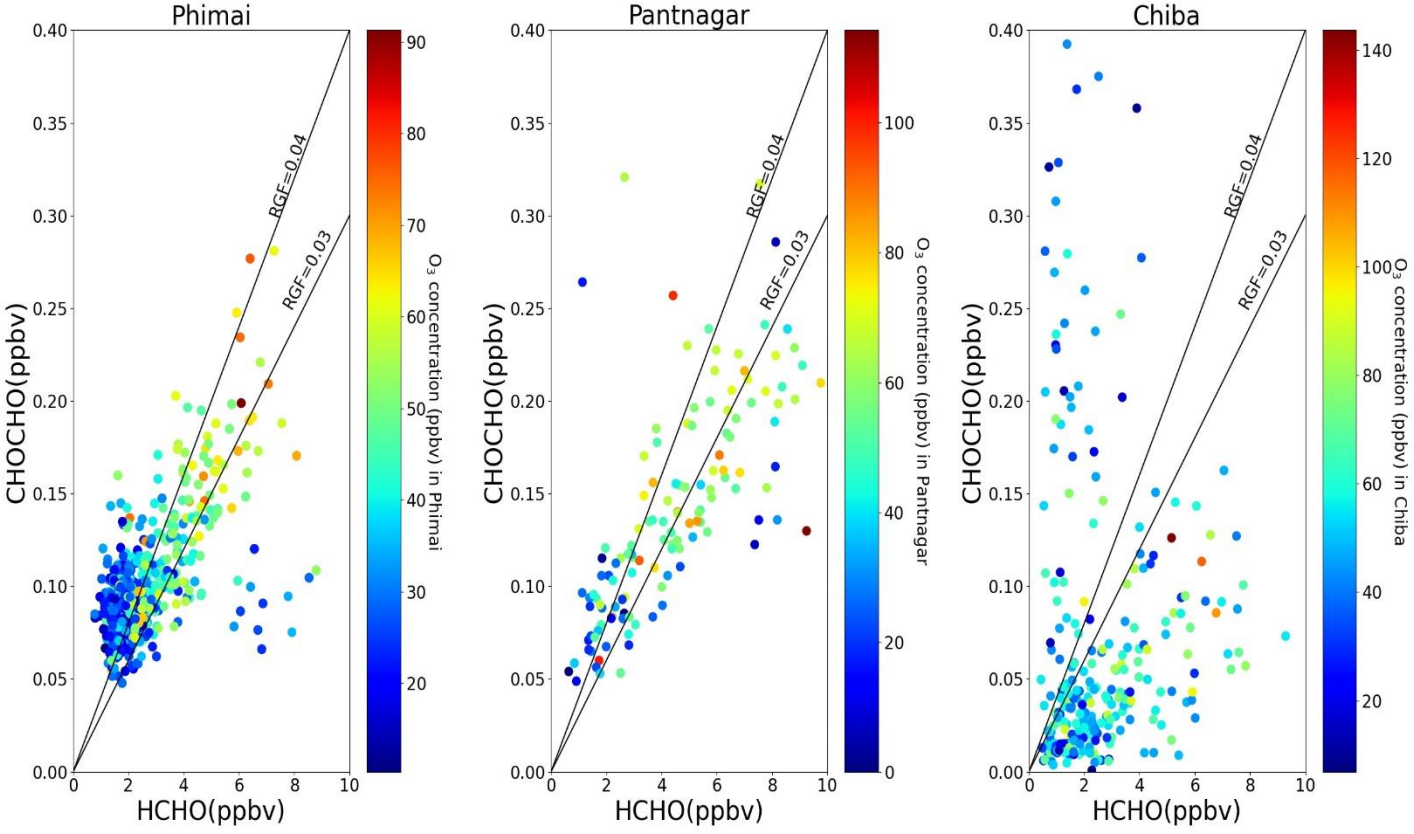

514 **Figure 7.** The scatter plots of CHOCHO and HCHO concentrations in the 0-1 km layer at Phimai, Pantnagar, and
515 Chiba, coloured with the O_3 concentrations in the 0-1 km layer at the respective sites. The solid lines indicate the
516 R_{GF} values at 0.04 and 0.03, respectively.
517
518
519
520
521

https://doi.org/10.5194/acp-2021-815
Preprint. Discussion started: 25 October 2021


Atmospheric Chemistry and Physics Discussions

522 **3.2 MAX-DOAS and CHASER comparison**

523 **3.2.1 Comparison between MAX-DOAS and CHASER HCHO**

524 Figure 8 shows seasonal averages of the HCHO profiles and partial columns (1–4 km) at the three
525 SKYNET sites for the MAX-DOAS and CHASER datasets. In addition, the CHASER outputs smoothed
526 with MAX-DOAS averaging kernels (AK) are depicted. The AK was applied following the procedure
527 described by Franco et al. (2015). First, the CHASER HCHO profiles were interpolated to the MAX-
528 DOAS vertical grids. Then the averaging AK was applied to the daily mean interpolated profiles. Next,
529 the MAX-DOAS AK information from individual retrieved profiles was seasonally averaged according
530 to the climate classifications of each site. Finally, the CHASER output for the days when observations
531 are available was selected for the comparison. The numbers of days available for comparison at Phimai,
532 Pantnagar, and Chiba were, respectively, 690, 340, and 668.

533 At the Phimai and Chiba sites, the HCHO partial columns of both datasets agree well within the 1σ
534 standard deviation of the MAX-DOAS observations. The HCHO partial column's enhancement because
535 of biomass burning in Phimai during the dry season was captured by CHASER. The HCHO profiles of
536 both datasets also show good agreement at the Chiba and Phimai sites. In both datasets, the peak
537 concentration of HCHO during the dry season in Phimai is ~5 ppbv, indicating that the biomass burning
538 estimates used in CHASER are reasonable. At both sites, CHASER has exhibited good skill at
539 reproducing HCHO concentrations below 2 km. Actually, CHASER simulates slightly lower HCHO
540 concentrations than MAX-DOAS at the Chiba site and overestimates HCHO during the wet season in
541 Phimai. However, CHASER HCHO profiles are mainly within the 1σ standard deviation range of the
542 ground-based observations. Application of AK to the CHASER profiles improves agreement between the
543 datasets, as Table 3 shows. At both sites, however, larger discrepancies are observed above 2 km. Such
544 differences are expected because of the reduced sensitivity of MAX-DOAS in the upper tropospheric
545 layers.

https://doi.org/10.5194/acp-2021-815
Preprint. Discussion started: 25 October 2021

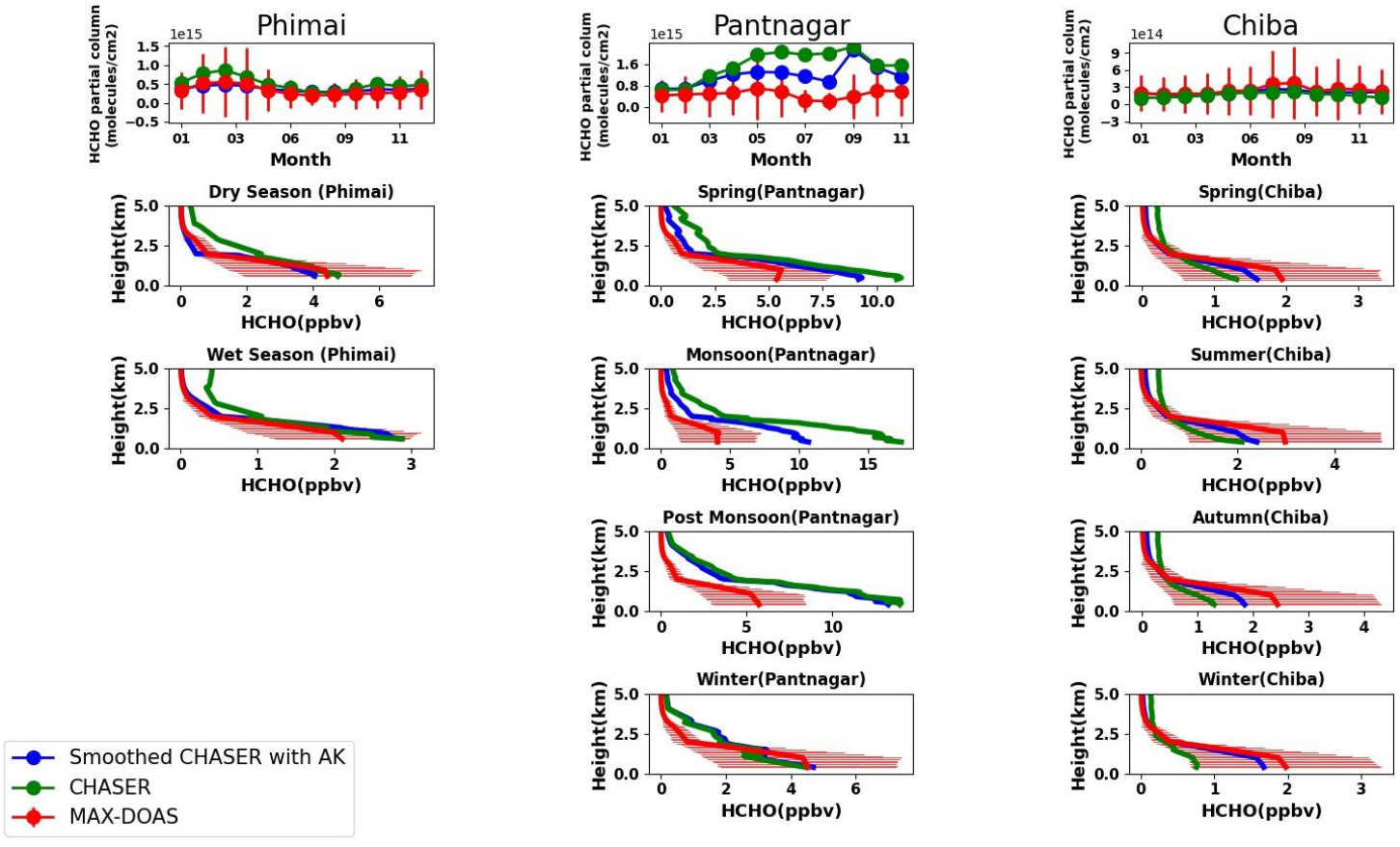

Figure 8. The seasonal variations in the HCHO partial columns from 1 to 4 km and vertical profiles during all seasons at the three A-SKY sites, inferred from the MAX-DOAS observations (red) and CHASER simulation(green). The CHASER HCHO partial column and vertical profile smoothed with the MAX-DOAS AK are shown in blue colour. The AK information of all the screened (as explained in section 2.2) retrievals was averaged based on the respective sites' seasonal classification. The selected CHASER simulated time and date corresponds to the available MAX-DOAS observations at the individual sites. The error bars indicate the one sigma standard deviation of mean values of the MAX-DOAS observations.

https://doi.org/10.5194/acp-2021-815
Preprint. Discussion started: 25 October 2021


Atmospheric Chemistry and Physics Discussions

558 **Table 3:** The seasonal differences between the observed and modelled HCHO concentrations in the 0-1
559 km layer in Phimai and Chiba. The units of the differences are given in ppbv.

Site	Season	MAX-DOAS – CHASER	MAX-DOAS – smoothed CHASER
Phimai	Dry	-0.34	-0.12
Phimai	Wet	-0.68	-0.31
Chiba	Spring	0.96	0.71
Chiba	Summer	-0.02	-0.10
Chiba	Autumn	-0.38	-0.22
Chiba	Winter	0.27	-0.05

560
561
562 At the Pantnagar site, considerable discrepancies were found between data of CHASER and MAX-
563 DOAS, mainly during the monsoon and post-monsoon seasons. During the monsoon season, CHASER-
564 simulated HCHO concentrations show a peak. The comparison results did not improve despite application
565 of AK to the CHASER output. In most cases, the CHASER simulated values are almost twice the
566 observation values. To infer the potential reason for the discrepancies, the annual mean HCHO
567 concentrations at all three sites are shown in Figure 9. CHASER-simulated HCHO concentrations at
568 Phimai and Pantnagar are similar, consistent with the MAX-DOAS observations at both locations (Fig.
569 1). Consequently, emission estimates used in the CHASER simulations are unlikely to contribute to the
570 marked discrepancies found for the comparison at Pantnagar. Mountainous terrain exists a few kilometers
571 away from the Pantnagar site. The differences can originate from treatment of the complex landscapes in

https://doi.org/10.5194/acp-2021-815
Preprint. Discussion started: 25 October 2021

Atmospheric Chemistry and Physics Discussions

572 the retrieval and simulations. The radiative transfer calculations for MAX-DOAS retrieval consider a flat
573 terrain. Such an assumption is expected to have a non-significant effect on retrieval because the horizontal
574 resolution of the MAX-DOAS system is ~10 km.
575

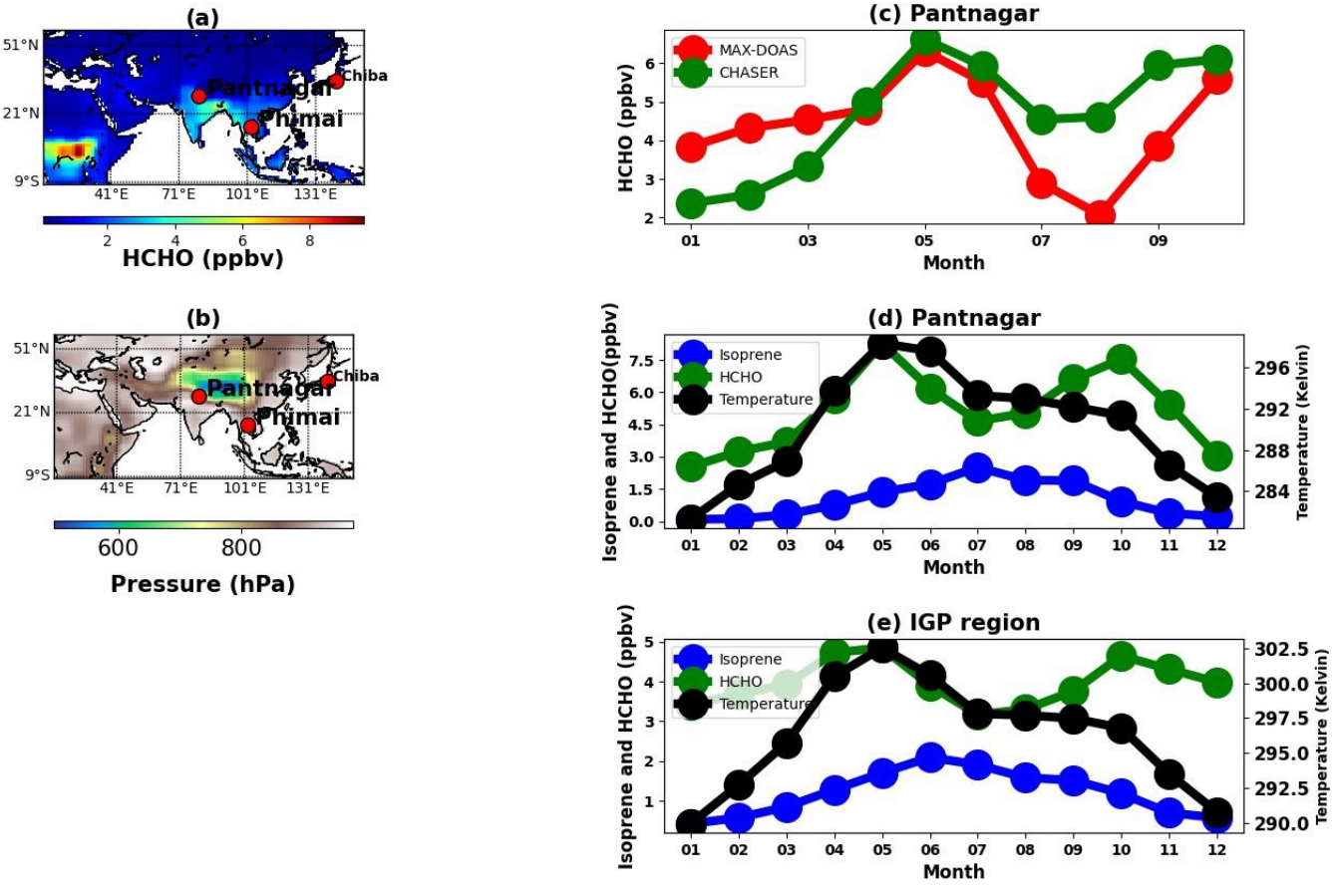

576

577 **Figure 9.** (left panel) **(**a) The mean surface HCHO concentrations at the three SKYNET sites in 2017, simulated
578 by CHASER. (b) The simulated mean surface pressure at the respective SKYNET sites. (right panel) (c) The
579 seasonal variations in the MAX_DOAS (red) and CHASER (green) HCHO concentrations in Pantnagar. The
580 coincident dates between the observations and model are plotted only. The CHASER simulated seasonal variations
581 in HCHO (green), isoprene (blue), and temperature (black) in 2017 in (d) Pantnagar and (e) the IGP region. Only
582 the daytime simulated values were used for the plots (a), (b), (d), and (e).
583

https://doi.org/10.5194/acp-2021-815
Preprint. Discussion started: 25 October 2021


Atmospheric Chemistry and Physics Discussions

584

585 Moreover, the MAX-DOAS HCHO products in Pantnagar showed good agreement with satellite
586 observations (Hoque et al., 2018b). Figure 9b shows the CHASER simulated surface pressure results
587 obtained for all three sites. The lower surface pressure at Pantnagar, compared to the other sites, indicates
588 that the surface elevation of Pantnagar is higher because of the mountains around the site. The simulated
589 surface height at Pantnagar is ~1700 m, although it is ~300 m in Phimai and Chiba. Consequently, when
590 CHASER values at Pantnagar are extrapolated to the MAX-DOAS grid (~100 m), the surface HCHO
591 concentrations are considerably different from the observations. The CHASER HCHO simulation at
592 Pantnagar is compared directly with the MAX-DOAS observations, as depicted in Fig. 9(c). Only the
593 coincident days between the observation and model are shown.

594 The HCHO seasonal variations in Pantnagar during the winter and spring are well reproduced by
595 CHASER. The peak HCHO concentrations during spring are ~6 ppbv in both datasets. The most marked
596 discrepancies occurred during the monsoon season, during which CHASER values are largely
597 overestimated. To infer the potential reason for the discrepancy between the model and observation,
598 CHASER simulated isoprene concentrations, temperature, and HCHO concentrations at the Pantnagar
599 site, as depicted in Fig. 9(d).

600 Oxidization of precursor hydrocarbon and photochemical reactions are the most dominant sources of
601 HCHO. Isoprene is the most abundant hydrocarbon in the atmosphere. The average ambient isoprene
602 concentrations during July, August, and September in the IGP region are 1.4+0.3 ppbv (Mishra et al.,
603 2020). Therefore, a CHASER isoprene concentration range of 3–4 ppbv during the monsoon season seems
604 reasonable. The high concentrations of HCHO during the monsoon season coincide with the high isoprene
605 concentrations and temperature in Pantnagar. The tight correlation between the isoprene and HCHO
606 concentrations suggests that the CHASER simulated HCHO at Pantnagar is governed by the isoprene
607 seasonal modulation. Also, MAX-DOAS HCHO concentrations are lower during the monsoon season,
608 likely because of the strong wet deposition and suppressed photochemical activities. Consequently, the
609 physical processes driving the HCHO concentration at Pantnagar in the second half of a year differ from
610 those considered in the model.

https://doi.org/10.5194/acp-2021-815
Preprint. Discussion started: 25 October 2021


Atmospheric Chemistry and Physics Discussions

611 Surl et al. (2018) found good agreement between OMI and GEOS-CHEM HCHO columns in the IGP
612 region only during the first half of the year. The HCHO, isoprene, and temperature variations in the whole
613 IGP region are shown in Fig. 9(e). Reportedly, the HCHO concentrations in the IGP region reach a peak
614 during the spring and post-monsoon seasons. Strong correlation between HCHO, isoprene, and
615 temperature variation in the first half of the year indicates that the change in biogenic emissions strongly
616 drives the HCHO seasonal modulation. During the post-monsoon period, it is likely that biomass burning
617 and anthropogenic emissions are more dominant than biogenic emissions because HCHO modulation
618 differs from those of isoprene and temperature. CHASER simulations show low HCHO concentrations
619 in the IGP region during the monsoon despite high isoprene concentrations and temperature. The HCHO
620 seasonal variation in the IGP is similar to that reported by Mahajan et al. (2015), which indicates that the
621 physical processes driving the HCHO seasonality in the IGP region are well reflected in the CHASER
622 simulations. Consequently, the assumptions of CHASER simulations (i.e., emissions and physical
623 processes) are unlikely to be an important reason for the discrepancy in the comparison for Pantnagar.
624 Because CHASER demonstrated good capability to reproduce the HCHO seasonal variation at a regional
625 scale (i.e., in the IGP region), the discrepancies at the local scale comparison (i.e., in Pantnagar) are
626 expected to decrease with high resolution (improved spatial resolution) simulations.
627
628 **3.2.2 Comparison between MAX-DOAS and CHASER NO_2**
629 Figure 10 presents the seasonal averages of the NO_2 profiles and partial columns (<4 km) at the Phimai
630 and Chiba sites for the MAX-DOAS and CHASER datasets. Calculation of the smoothed CHASER
631 output is similar to that explained in the section 3.2.2. Data of comparisons in Phimai and Chiba are
632 presented in Table 4. The smoothed CHASER NO_2 partial column and profiles show good agreement
633 with the MAX-DOAS datasets at both locations. CHASER well reproduced the enhanced NO_2 during the
634 dry season in Phimai. Amidst the biomass burning influence, the NO_2 concentrations in Phimai are mostly
635 < 1 ppbv. Consequently, CHASER demonstrated good skills in a region characterized by low NO_2
636 concentrations (<1 ppbv). CHASER simulations do not show the NO_2 enhancement related to soil NO_x
637 emissions during the wet season. However, sensitivity studies with CHASER simulations quantified the
638 soil NOx contribution to the NO_2 concentrations in Phimai (Fig. 5). This result indicates that CHASER

https://doi.org/10.5194/acp-2021-815
Preprint. Discussion started: 25 October 2021

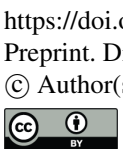

Atmospheric Chemistry and Physics Discussions

captured the soil NO_x contribution, but the magnitude differs because of the horizontal resolution of the datasets.

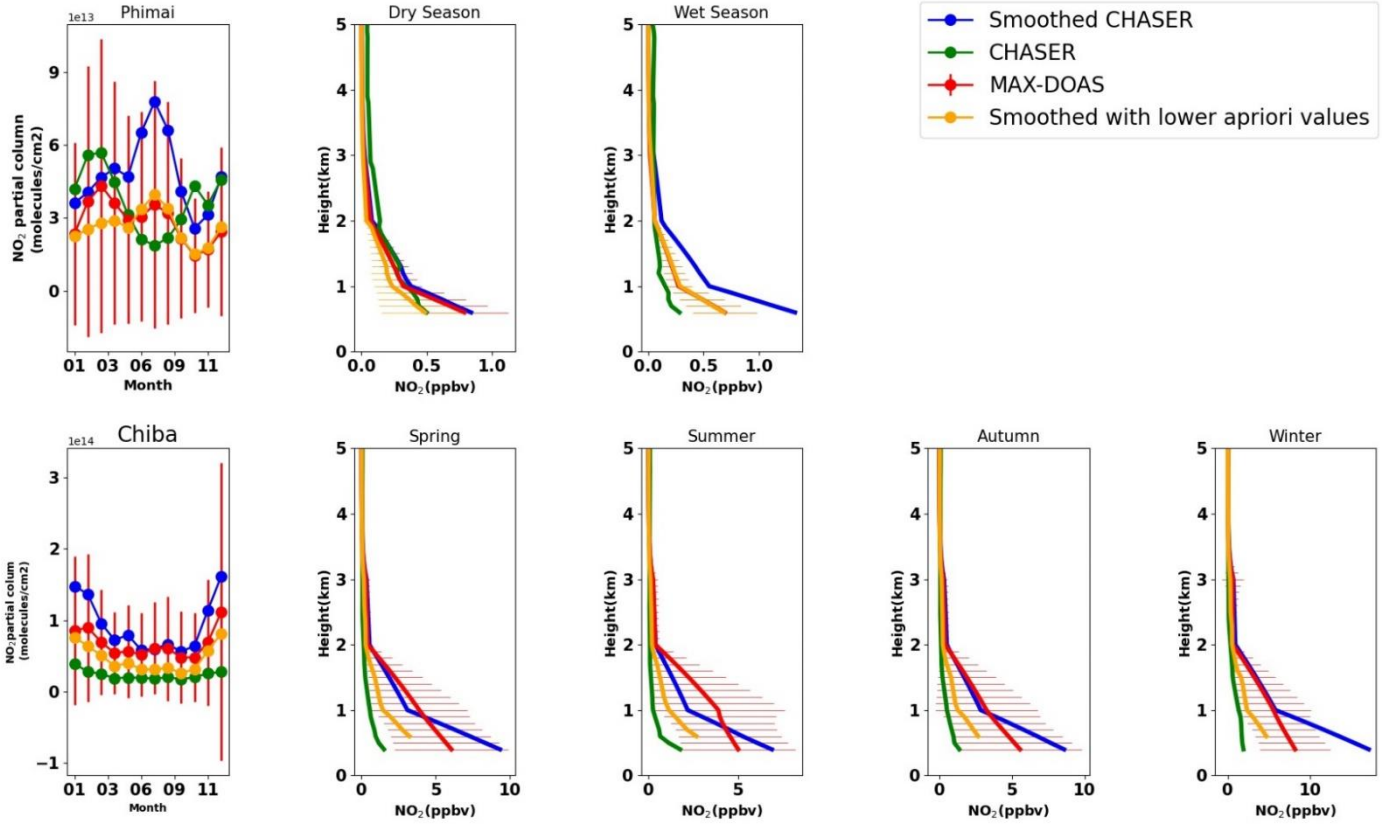

Figure 10. The seasonal variations in the NO_2 partial columns (< 4 km) and vertical profiles during all seasons at Phimai and Chiba, inferred from the MAX-DOAS observations (red) and CHASER simulation(green). The CHASER NO_2 partial columns and vertical profiles smoothed with the MAX-DOAS AK are shown in blue color. The orange colour indicates the smoothed CHASER profile when calculated with apriori values reduced by 50%. The AK information of all the screened (as explained in section 2.2) retrievals was averaged based on the respective sites' seasonal classification. The selected CHASER simulated time and date corresponds to the available MAX-DOAS observations at the respective sites. The error bars indicate the one sigma standard deviation of mean values of the MAX-DOAS observations.

https://doi.org/10.5194/acp-2021-815
Preprint. Discussion started: 25 October 2021


Atmospheric Chemistry and Physics Discussions

652

653 **Table 4:** The seasonal differences between the observed and modelled NO_2 concentrations in the 0-1 km
654 layer in Phimai and Chiba. The unit of the differences are in ppbv.

Site	Season	MAX-DOAS – CHASER	MAX-DOAS – smoothed CHASER
Phimai	Dry	-0.12	-0.17
Phimai	Wet	-0.02	-0.70
Chiba	Spring	2.69	-0.91
Chiba	Summer	2.70	-0.30
Chiba	Autumn	2.21	-1.02
Chiba	Winter	2.21	-1.71

655

656

657 Results show that CHASER underestimated the NO_2 concentration in Chiba, although the smoothed
658 CHASER output agrees well with observations. The simulated values were mainly within one sigma
659 standard deviation of the MAX-DOAS values. At both sites, smoothed NO_2 profiles at 0–2 km were in
660 good agreement with observations. Although the smoothed output improved the comparison results, the
661 variation in the smoothed output differed from the model output, mostly during all seasons in Chiba and
662 during the wet season in Phimai. Such differences are likely to be related to the apriori data used for
663 smoothing the CHASER output. Figure 10 includes the smoothed output produced when a priori values
664 are decreased by 50%. The a priori data used to retrieve the profile information are taken from the
665 retrieved VCD and SCD values. Because MAX-DOAS observations are most sensitive to the lower

https://doi.org/10.5194/acp-2021-815
Preprint. Discussion started: 25 October 2021


Atmospheric Chemistry and Physics Discussions

tropospheric layers, the apriori values affected the smoothed model output, mostly within the 0–2 km layers. Therefore, the discrepancies between CHASER and smoothed CHASER profiles are lessened when lower apriori values are used. The overestimated values in the smoothed output during the wet season in Phimai and spring and winter in Chiba were also improved when lower apriori values were used. Although the apriori values primarily affect the smoothed profile shapes, that variation is mostly within 1σ standard deviation of the observations. At Phimai, the model output shows better agreement with observations than that found for the smoothed outputs. At a low NO_2 concentration concentration (< 1 ppbv), the AK information seems to be less significant if the model can reproduce low concentration scenarios.

Based on the discussion of HCHO comparisons in Pantnagar, CHASER-simulated NO_2 concentrations at Pantnagar are compared directly with observations depicted in Fig. 11. The NO_2 seasonal variation in the datasets disagrees considerably. To infer the potential reasons for the disagreement, the NO_2 simulations in the whole IGP region and the simulations around two megacities in the IGP region, New Delhi and Kolkata, are shown in the figure. In addition, NO_2 surface measurements in the megacities reported by Malik and Lal (2015) are considered. The lowest concentrations during the monsoon characterize the overall NO_2 variation in the IGP. The CHASER NO_2 simulations show similar seasonal modulation in both cities. The observed and modeled NO_2 seasonal variability in New Delhi and Kolkata agree well with *R* values of 0.80 despite the underestimated model values. To improve the agreement in terms of absolute values, simulations with optimized anthropogenic emissions are conducted and presented in Figs. 11(c) and 11(d). Increasing the anthropogenic emissions improves the agreement between the model and observations, mostly in New Delhi. On a seasonal scale, the maximum change in the NO_2 concentration in the megacities are between 10–20 and 15–25 ppbv, according respectively to the observations and model. Consequently, despite underestimation, the CHASER NO_2 simulations seem reasonable.

https://doi.org/10.5194/acp-2021-815
Preprint. Discussion started: 25 October 2021

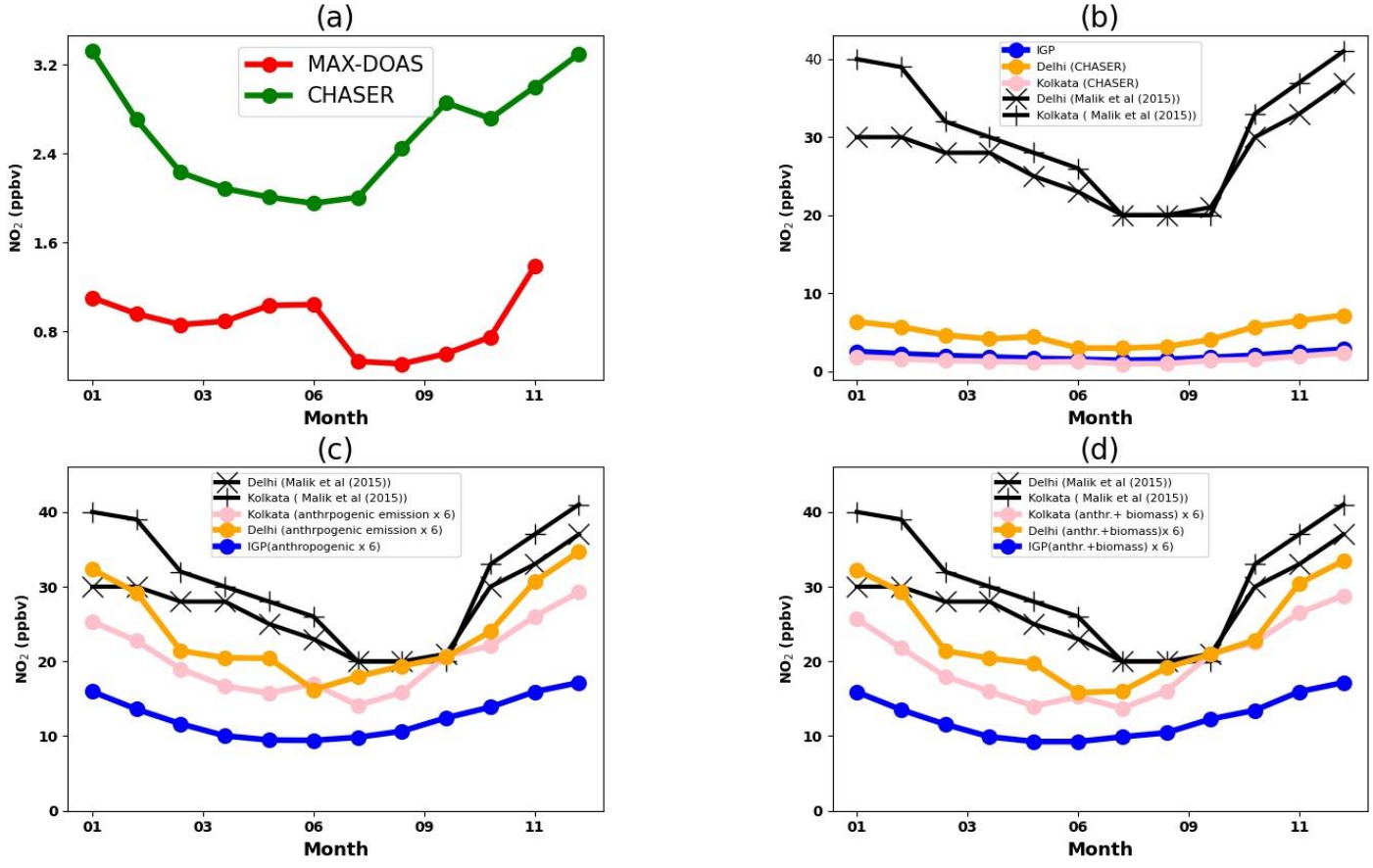

Figure 11. (a) The seasonal variation in the NO2 concentrations in the 0-1 km layer in Pantnagar was obtained from the MAX-DOAS observations (red) and CHASER simulations (green). The coincident dates between the datasets were selected for the plot. (b) The CHASER simulated surface NO_2 concentrations in New Delhi, Kolkata, and the IGP region. New Delhi and Kolkata are two megacities located in the IGP region. The black curves show the surface NO_2 concentrations in New Delhi and Kolkata reported by Malik and Lal (2015). The CHASER simulated NO2 concentrations in the IGP region, New Delhi, and Kolkata (c) with increased anthropogenic emissions and (d) with increased anthropogenic and biomass burning emissions. The observational data in both (c) and (d) are taken from the work of Malik and Lal (2015)

https://doi.org/10.5194/acp-2021-815
Preprint. Discussion started: 25 October 2021


Atmospheric Chemistry and Physics Discussions

Similar results are obtained when biomass burning emissions are optimized and anthropogenic emissions (Fig. 11(d)) are included, indicating that the anthropogenic emissions' changes primarily drive the NO_2 variation found in the IGP region. In contrast, the NO_2 seasonality in Pantnagar is influenced strongly by biomass burning (according to observations), thereby leading to the discrepancy between the observations and model in Pantnagar. In the case of Pantnagar, the CHASER shows better skills at reproducing the climatology of NO_2 and HCHO on a regional scale.

3.2.3 Contribution from biomass burning to the HCHO and NO_2 abundances in Phimai and Pantnagar

This section presents estimation of the contribution of biomass to the HCHO and NO_2 concentrations in Phimai and Pantnagar. Figure 12 presents results of simulation L1_HCHO, L1_opt, and L1_NO_2. The simulation settings are shown in Table 2. For better readability, the switched-off emissions criterion is described in the legends of Fig. 12. All the plots present the mean concentrations in the 0–1 km layer. Biomass burning contributes ~10% to the HCHO concentrations in Phimai during the dry season. However, based on the observations, a more substantial effect of biomass burning is expected. During the wet season, the MAX-DOAS and CHASER HCHO concentrations are, respectively, ~2 and ~4 ppbv, indicating overestimation of the biogenic emissions in CHASER. Figure 12(b) shows the HCHO concentration obtained from simulation L1_opt and MAX-DOAS observations in 2017. In the L1_opt simulation setting, the biomass burning emissions were switched off; the biogenic emissions were optimized to reproduce results analogous to those obtained from observations made during the wet season. In the absence of biomass burning, the surface HCHO concentrations in Phimai would be ~2 ppbv, resulting in a biomass burning contribution of ~20–50% during the dry season. The observed interseason difference in the HCHO concentration in Phimai is ~60%. Consequently, the revised biomass burning contribution estimate is apparently more reasonable. Pyrogenic emissions contributions to the NO_2 concentrations in Phimai are ~10% during the dry season (Fig. 12(c)). Because the NO_2 concentrations are low in Phimai, the simulation during March, when the influence of biomass burning is highest, is used to derive a better contribution estimate. As depicted in Fig. 12(d), in the absence of biomass burning, the

https://doi.org/10.5194/acp-2021-815
Preprint. Discussion started: 25 October 2021

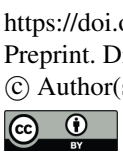

Atmospheric Chemistry and Physics Discussions

730 NO_2 concentration during March would be ~0.84 ppbv, indicating a contribution up to 35% to the NO_2
731 concentrations in Phimai.
732

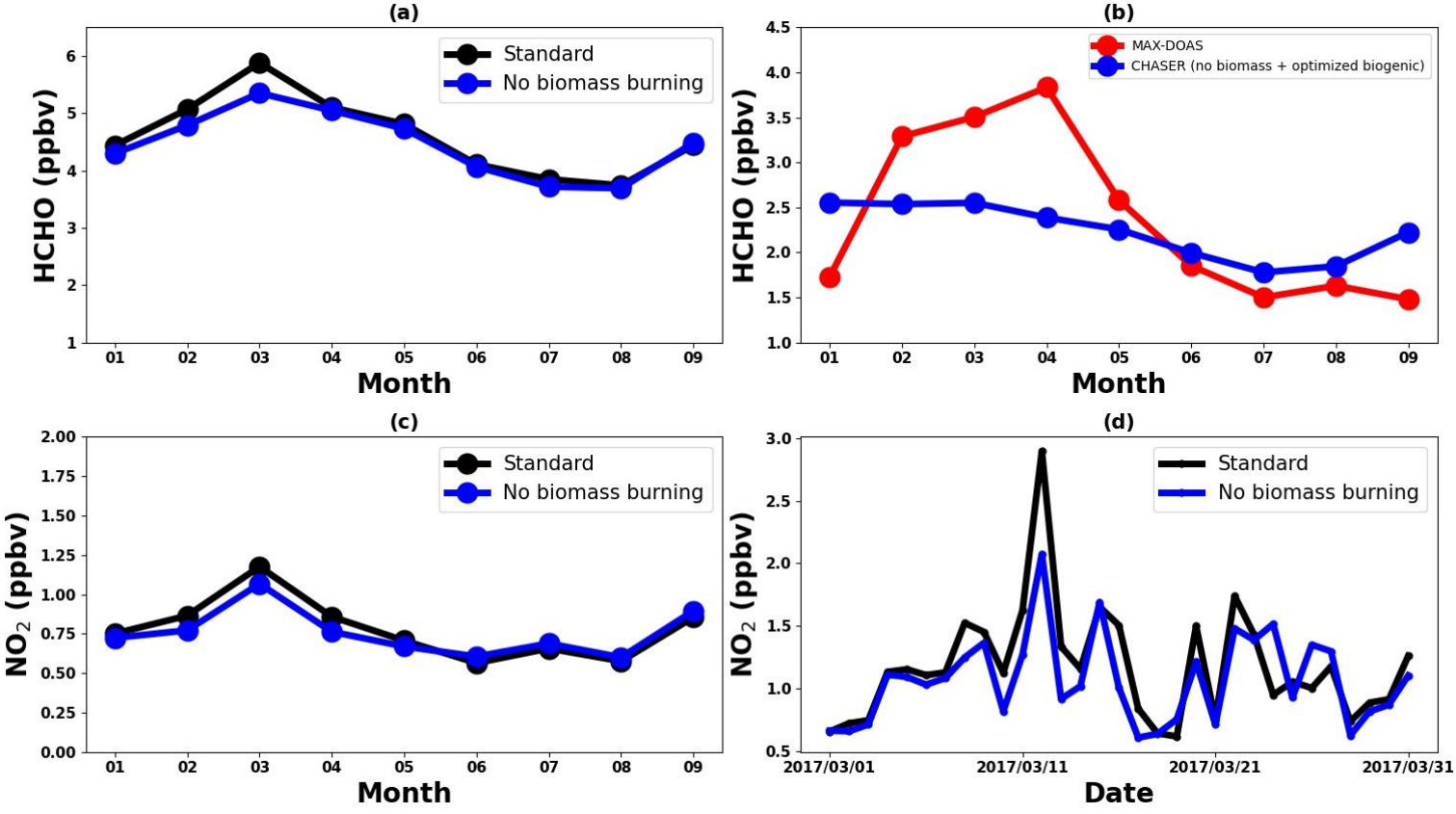

733

734 **Figure 12.** (top panel) The seasonal variations of the HCHO concentrations in the 0-1 km layer in Phimai, obtained
735 from the standard and L1_HCHO simulations. The pyrogenic emissions of VOCs are switched off in the L1_HCHO
736 simulations. (b) The HCHO seasonal variability in Phimai in 2017 was obtained from the MAX-DOAS
737 observations (red) and L1_opt simulations. In addition to switching off the pyrogenic VOC emissions, the biogenic
738 emissions were reduced by 50% in the L_opt simulation. The coincident dates between the observation and the
739 simulations are plotted only. (bottom panel) (c) The seasonal variation of NO_2 in Phimai was obtained from the
740 standard and L1_NO_2 simulations. The pyrogenic NO_2 emissions were switched off in the L1_NO2 simulations.
741 (d) The daily NO_2 concentrations in Phimai during March, obtained from the standard and L1_NO_2 simulations.

https://doi.org/10.5194/acp-2021-815
Preprint. Discussion started: 25 October 2021


Atmospheric Chemistry and Physics Discussions

742 All the simulations are plotted for the year 2017, and only the daytime values from 09:00 – 15:00 LT are used for
743 calculating the seasonal mean.
744
745
746 At Pantnagar, pyrogenic emissions contribute up to 13% to the HCHO concentrations, which is
747 apparently underestimated based on the observed seasonality (Fig. 13(a)). Because CHASER showed
748 better capability on a regional scale, the effect of pyrogenic emissions on the HCHO variation in the IGP
749 region is considered. According to L1_HCHO simulation results, the effect of biomass burning emissions
750 on the regional HCHO modulation is also apparently non-significant. The HCHO concentrations in India
751 have biogenic, anthropogenic, and pyrogenic VOC sources. Biogenic VOCs are the primary driver of the
752 over HCHO variation (Surl et al., 2018). Consequently, two potential reasons might be responsible for
753 small effects of pyrogenic emissions on HCHO concentrations: (1) Overestimation of the biogenic
754 emission or underestimation of pyrogenic emissions in the model. (2) Stronger effects of anthropogenic
755 VOC emissions than those of pyrogenic VOCs. In fact, CHASER overestimated the HCHO
756 concentrations at both sites, indicating overestimation of biogenic emissions. To infer the role of
757 anthropogenic emissions on the HCHO concentration, the results of simulation L2 are depicted in Figs.
758 13(a) and 13(b). Anthropogenic emissions contribute up to 30% of the HCHO concentration in the IGP
759 region, with a maximum contributed during the post-monsoon season. The greatest effect of
760 anthropogenic emissions during the post-monsoon seasons coincides with the lower isoprene
761 concentration (i.e., biogenic emissions) and temperature (Fig. 9(e)). Consequently, anthropogenic
762 emissions are likely to be a significant driver of HCHO concentrations in the IGP region after biogenic
763 emissions. At Pantnagar, anthropogenic VOCs contribute more (~. 30%) than pyrogenic emissions do.
764 It is particularly interesting that during the spring, CHASER simulations show that biomass burning
765 contributes up to 8% and 15% to the NO_2 concentrations, respectively, in Pantnagar and the IGP region
766 (Fig. 13(c)). According to results reported by Hoque et al. (2018b), biomass burning is expected to have
767 a stronger influence on NO_2 and HCHO climatology in Pantnagar. A reasonable estimate of the
768 contributions from different emission sources in Pantnagar can likely be obtainable from higher resolution
769 CHASER simulations. However, the regional contribution estimates are reasonable.

https://doi.org/10.5194/acp-2021-815
Preprint. Discussion started: 25 October 2021

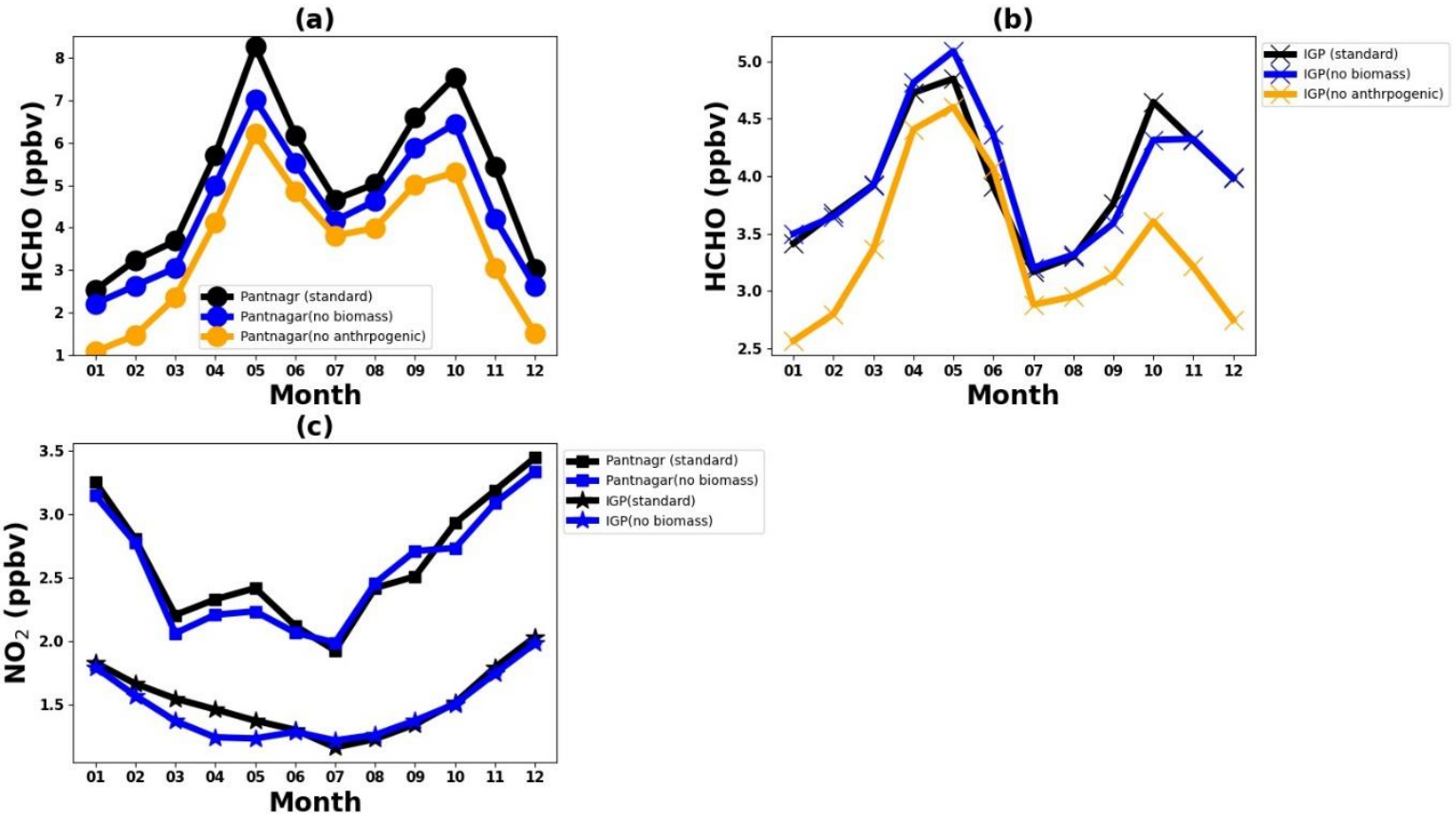

Figure 13. The seasonal variations of the HCHO concentrations in the 0-1 km layer in (a)Pantnagar and (b) in the IGP region, obtained from the standard, L1_HCHO, and L2 simulations. VOCs' pyrogenic emissions and anthropogenic emissions are switched off in the L1_HCHO and L2 simulations, respectively. (c) The seasonal variation of NO_2 in Pantnagar and the IGP region was obtained from the standard and L1_NO_2 simulations. The pyrogenic NO_2 emissions were switched off in the L1_NO2 simulations. All the simulations are plotted for the year 2017. All the simulations are plotted for the year 2017, and only the daytime values from 09:00 – 15:00 LT are used for calculating the seasonal mean.

3.2.4 Comparison between CHASER and MAX-DOAS R_{FN} values:

https://doi.org/10.5194/acp-2021-815
Preprint. Discussion started: 25 October 2021

Atmospheric Chemistry and Physics Discussions

782 Scatter plots of the CHASER and MAX-DOAS HCHO and NO_2 abundances in the 0–3 km layer of the
783 troposphere color-coded with MAX-DOAS O_3 concentrations for the Phimai and Pantnagar site are
784 depicted in Fig. 14. This discussion excludes the Pantnagar site because of challenges that hinder
785 application of the AK, as discussed in section 3.2.1. The O_3 production regime in Phimai is NO_x limited.
786 Also, CHASER produced similar results for the Phimai site, with high O_3 concentrations associated
787 primarily with NO_2 concentrations < 0.4 ppbv. Some discrepancies were found between CHASER and
788 MAX-DOAS NO_2 abundances during the wet season, leading to differences in the absolute R_{FN} values.
789 Such discrepancies in R_{FN} values are minimized by smoothing the CHASER output with that of the MAX-
790 DOAS AK.

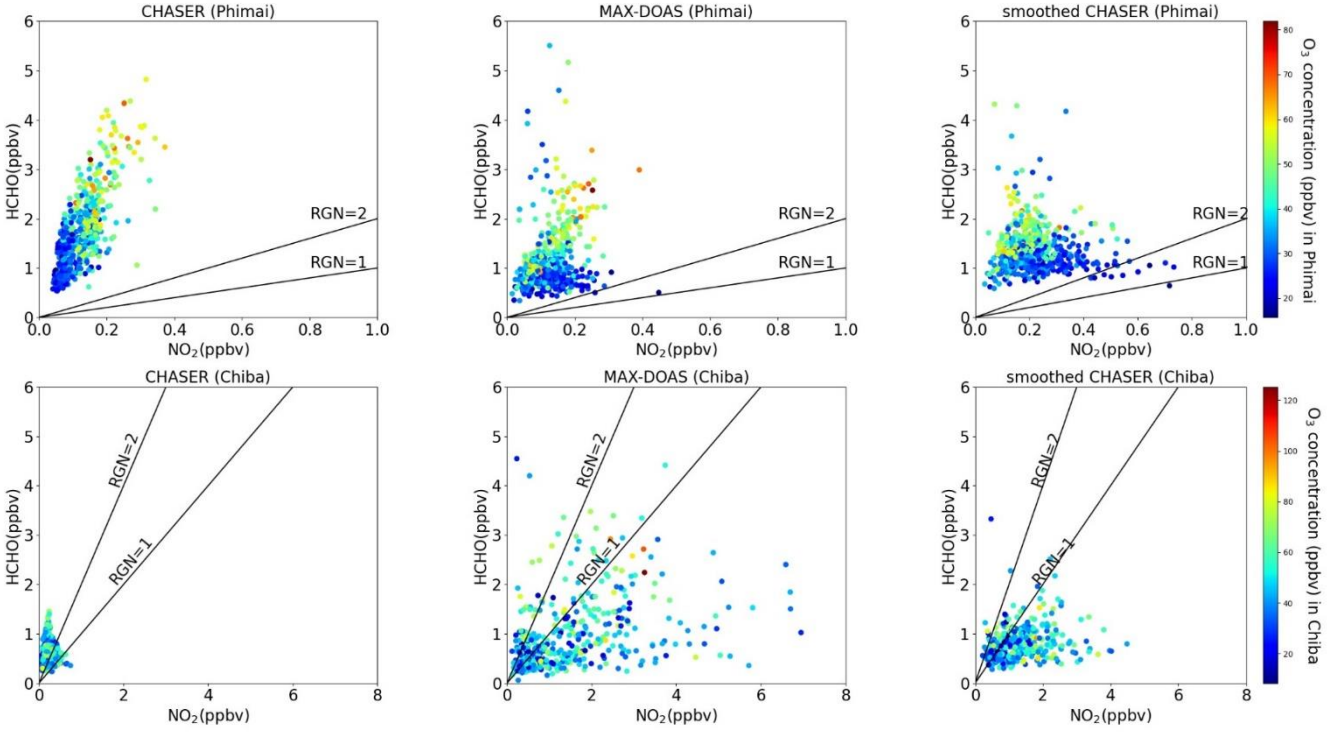

791
792
793 **Figure 14.** The scatter plots of the daily mean HCHO and NO_2 concentrations in the 0-3 km layer at Phimai and
794 Chiba, inferred from MAX-DOAS observations, CHASER simulations, and smoothed CHASER output (with
795 MAX-DOAS AK), coloured with the daily mean O_3 concentrations in the 0- 3 km layer retrieved from the MAX-

https://doi.org/10.5194/acp-2021-815
Preprint. Discussion started: 25 October 2021


Atmospheric Chemistry and Physics Discussions

DOAS observations at the respective sites. The solid lines indicate the R_{GN} values at 2 and 1, respectively. In addition, the time and date of the CHASER simulation, which coincides with the MAX-DOAS observations at the respective sites were selected.

At the Chiba site, CHASER and MAX-DOAS R_{FN} values differ considerably, indicating the O_3 production regime. The smoothed CHASER output shows that the R_{FN} values are mostly lower than 1, which is indicative of a VOC limited region, consistent with the observations and the results reported by Irie et al. (2021). At the Chiba site, there are days (~80) when the O_3 sensitivity lies in the transition region (i.e., $1<R_{FN}<2$). However, the R_{FN} values were less than unity most days (~280), suggesting a dominant VOC limited region.

Conclusions

MAX-DOAS observations were made at three A-SKY sites from January 2017 through December 2018. Also, NO_2 and HCHO concentrations and profiles were retrieved using the JM2 algorithm. The retrieved products were compared with those of simulations obtained using the global chemistry transport model CHASER. At all three sites, the seasonal variation of both trace gases was consistent throughout the investigated period. At Phimai and Pantnagar, biomass burning led to enhanced HCHO and NO_2 concentrations, respectively, during the dry season and spring and post-monsoon season. Both the model and observations confirmed the contribution of soil NO_x emissions to the NO_2 concentrations in Phimai. The R_{FN} ratio estimated from the observations showed that the O_3 production regime in Phimai and Pantnagar was NOx limited, whereas the O_3 production in Chiba was governed primarily by the NO_x emissions (VOC limited). The observed and modeled R_{FN} ratios estimated for the Phimai and Chiba sites

https://doi.org/10.5194/acp-2021-815
Preprint. Discussion started: 25 October 2021


Atmospheric Chemistry and Physics Discussions

were consistent. CHASER demonstrated good capability for reproducing the HCHO seasonal variation at Phimai and Chiba. Although the HCHO datasets for the Pantnagar site showed discrepancies, the modeled HCHO seasonal variation in the IGP region was consistent with values found in the literature, indicating that the differences were related mainly to the model's coarse resolution.

Moreover, general overestimation was made of the biogenic emissions in the model. The observed and modeled NO_2 variation in Phimai and Chiba showed good agreement. However, the a priori values had a marked effect on the smoothed model output. In Phimai, the biomass burning contributions to the HCHO and NO_2 concentrations were up to ~50 and ~ 35%, respectively, whereas, in Pantnagar, the pyrogenic contributions were ~13 and ~8%, respectively. The estimates for Pantnagar were underestimated, as inferred from observationally obtained evidence, which can be improved with model simulations at higher spatial resolution. Anthropogenic emissions were revealed as an important driver of the VOC variation in the IGP region after biogenic emissions, which is consistent with findings reported in the literature.

Code availability. The CHASER and JM2 source codes are not available publicly. Dr. Kengo Sudo (kengo@nagoya-u.jp) is the contact person for readers and researchers interested in the CHASER model. In addition, Dr. Hitoshi Irie (hitoshi.irie@chiba-u.jp) will answer queries regarding the usage of the JM2 codes.

Data availability: The MAX-DOAS data used in the study are publicly accessible on the A-SKY network website (http://atmos3.cr.chiba-u.jp/a-sky/data.html). The corresponding author can provide the CHASER simulations and MAX-DOAS averaging kernel data upon request.

https://doi.org/10.5194/acp-2021-815
Preprint. Discussion started: 25 October 2021

Atmospheric Chemistry and Physics Discussions

Author contributions: HMSH conceptualized the study, conducted the model simulations, analyzed the data, and drafted the manuscript. AMF helped with the data processing. HI developed the JM2 code and maintained the A-SKY network. KS developed the CHASER model and supervised the study. AD shared his experience to explain the results. HI, KS, AD, and AMF commented and provided feedback on the final results and manuscript.

Conflict of Interest: The authors declare that they have no conflict of Interest

Acknowledgments: This research is supported by the Global Environmental Research fund (S-12 and S-20) of the Ministry of the Environment (MOE), Japan, and JSPS KAKENHI Grants: JP20H04320, JP19HO5669, and JP19H04235. The CHASER model simulations are partly performed with the supercomputer (NEC SX-Aurora TSUBASA) at the National Institute for environmental studies (NIES), Tsukuba, Japan.

References

Arlander, D., Brüning, D., Schmidt, U., and Ehhalt, D. : The tropospheric distribution of formaldehyde during TROPOZ II, J. Atmos. Chem., 22(3), 251-269, https://doi.org/10.1007/BF00696637, 1995

Biswas, M. S., Ghude, S. D., Gurnale, D., Prabhakaran, T., and Mahajan, A. S. : Simultaneous Observations of Nitrogen Dioxide, Formaldehyde and Ozone in the Indo-Gangetic Plain. Aerosol Air Qual. Res., 19(8), 1749-1764, https://doi.org/10.4209/aaqr.2018.12.0484, 2019

Bond, D. W., Zhang, R., Tie, X., Brasseur, G., Huffines, G., Orville, R. E., and Boccippio, D. J. : NO_x production by lightning over the continental United States, J. Geophys. Res., 106(D21), 27701-27710, https://doi.org/10.1029/2000JD000191, 2001

Burkert, J., Andrés-Hernández, M. D., Stöbener, D., Burrows, J. P., Weissenmayer, M., & Kraus, A. (2001) : Peroxy radical and related trace gas measurements in the boundary layer above the Atlantic Ocean, J. Geophys. Res., 106(D6), 5457-5477, https://doi.org/10.1029/2000JD900613, 2001

Cárdenas, L., Rondón, A., Johansson, C., & Sanhueza, E. : Effects of soil moisture, temperature, and inorganic nitrogen on nitric oxide emissions from acidic tropical savannah soils. J. Geophys. Res., 98(D8), 14783-14790, https://doi.org/10.1029/93JD01020, 1993

Chaliyakunnel, S., Millet, D. B., and Chen, X. : Constraining emissions of volatile organic compounds over the Indian subcontinent using space-based formaldehyde measurements. J. Geophys. Res., 124(19), 10525-10545, https://doi.org/10.1029/2019JD031262, 2019

Clémer, K., Van Roozendael, M., Fayt, C., Hendrick, F., Hermans, C., Pinardi, G., Spurr, R., Wang, P., and De Mazière, M. : Multiple wavelength retrieval of tropospheric aerosol optical properties from MAXDOAS measurements in Beijing, Atmos. Meas. Tech., 3(4), 863-878, https://doi.org/10.5194/amt-3-863-2010, 2010

Colella, P., & Woodward, P. R. : The piecewise parabolic method (PPM) for gas-dynamical simulations. J. Comput. Phys., 54(1), 174-201, https://doi.org/10.1016/0021-9991(84)90143-8, 1984

Colliander, A., Jackson, T. J., Bindlish, R., Chan, S., Das, N., Kim, S., Cosh, M.H., Dunbar, R.S., Pashaian, L., Asanuma, J., Aida, K., Berg, A., Rowlandson, T., Bosch, D., Caldwell, T., Caylor, K., Goodrich, D., al Jassar, H., Lopez-Baeza, E., Martinez-Farnandez, J., Gonzalez-Zamora, A., Livingston, S., McNairn, H., Pacheco, A., Moghaddam, M., Montzka, C., Notarnicola, C., Niedirst, G., Pellarin, T., Prueger, J., Pulliainen, J., Rautiainen, K., Ramos, J., Seyfried, M., Starks, P., Su, Z., Yeng, Y., van der Velde, R., Thibeault, M., Dorigo, W., Vreugdenhil, M., Walker, J. p., Wu, X., Monerris, A., O'Neil, P.E., Entekhabi, D., Njoku, E.G., and Yueh, S. : Validation of SMAP surface soil moisture products with core validation sites. *Remote Sens. Environ,, 191*, 215-231, https://doi.org/10.1016/j.rse.2017.01.021, 2017

Crutzen, P. J. : The influence of nitrogen oxides on the atmospheric ozone content. Q. J. Roy. Meteor. Soc., 96(408), 320-325, https://doi.org/10.1002/qj.49709640815, 1970

Davidson, E. A., Vitousek, P. M., Matson, P. A., Riley, R., García-Méndez, G., & Maass, J. M. : Soil emissions of nitric oxide in a seasonally dry tropical forest of Mexico. *J. Geophys. Res.*, *96*(D8), 15439-15445, https://doi.org/10.1029/91JD01476, 1991

DiGangi, J. P., Henry, S. B., Kammrath, A., Boyle, E. S., Kaser, L., Schnitzhofer, R., Graus, M., Turnipseed, A., Park, J.-H., Weber, R. J., Hornbrook, R. S., Cantrell, C. A., Maudlin III, R. L., Kim, S., Nakashima, Y., Wolfe, G. M., Kajii, Y., Apel, E. C., Goldstein, A. H., Guenther, A., Karl, T., Hansel, A., and Keutsch, F. N.: Observations of glyoxal and formaldehyde as metrics for the anthropogenic impact on rural photochemistry. Atmos. Chem. Phys., 12(20), 9529-9543, https://doi.org/10.5194/acp-12-9529-2012, 2012

931 Duncan, B. N., Yoshida, Y., Damon, M. R., Douglass, A. R., and Witte, J. C. : Temperature dependence of factors
932 controlling isoprene emissions. Geophys. Res. Lett., 36(5), https://doi.org/10.1029/2008GL037090, 2009
933
934
935 Emori, S., Nozawa, T., Numaguti, A., & Uno, I. : Importance of cumulus parameterization for precipitation
936 simulation over East Asia in June. J. Meteorol. Soc. Jpn., 79(4), 939-947.
937 https://doi.org/10.2151/jmsj.79.939, 2001
938
939 Franco, B., Hendrick, F., Van Roozendael, M., Müller, J.-F., Stavrakou, T., Marais, E. A., Bovy, B., Bader, W.,
940 Fayt, C., Hermans, C., Lejuene, B., Pinardi, G., Sevais, C., and Mahieu, E. : Retrievals of formaldehyde
941 from ground-based FTIR and MAX-DOAS observations at the Jungfraujoch station and comparisons with
942 GEOS-Chem and IMAGES model simulations. Atmos. Meas. Tech., 8(4), 1733-1756,
943 https://doi.org/10.5194/amt-8-1733-2015, 2015
944
945 Fu, T. M., Jacob, D. J., Wittrock, F., Burrows, J. P., Vrekoussis, M., and Henze, D. K. : Global budgets of
946 atmospheric glyoxal and methylglyoxal, and implications for formation of secondary organic aerosols, J.
947 Geophys. Res., 113(D15), https://doi.org/10.1029/2007JD009505, 2008
948
949
950 Frieß, U., Monks, P. S., Remedios, J. J., Rozanov, A., Sinreich, R., Wagner, T., & Platt, U. : MAX-DOAS O4
951 measurements: A new technique to derive information on atmospheric aerosols: 2. Modeling studies. J.
952 Geophys. Res., 111(D14), https://doi.org/10.1029/2005JD006618, 2006
953
954 Frieß, U., Klein Baltink, H., Beirle, S., Clémer, K., Hendrick, F., Henzing, B., Irie, H., de Leeuw, G., Li, A.,
955 Moerman, M. M., van Roozendael, M., Shaiganfar, R., Wagner, T., Wang, Y., Xie, P., Yilmaz, S., and
956 Zieger, P. : Intercomparison of aerosol extinction profiles retrieved from MAX-DOAS measurements.
957 Atmos. Meas.Tech., 9(7), 3205-3222, https://doi.org/10.5194/amt-9-3205-2016, 2016
958
959
960

Hak, C., Pundt, I., Trick, S., Kern, C., Platt, U., Dommen, J., Ordóñez, C., Prévôt, A. S. H., Junkermann, W., Astorga-Lloréns, C., Larsen, B. R., Mellqvist, J., Strandberg, A., Yu, Y., Galle, B., Kleffmann, J., Lörzer, J. C., Braathen, G. O., and Volkamer, R. : Intercomparison of four different in-situ techniques for ambient formaldehyde measurements in urban air, *Atmos. Chem. Phys.*, *5*(11), 2881-2900. https://doi.org/10.5194/acp-5-2881-2005, 2005

Hall, S. J., Matson, P. A., and Roth, P. M. : NO_x emissions from soil: implications for air quality modeling in agricultural regions. Annu. Rev. Energy Environ., 21(1), 311-346. https://doi.org/10.1146/annurev.energy.21.1.311, 1996

Halla, J. D., Wagner, T., Beirle, S., Brook, J. R., Hayden, K. L., O'Brien, J. M., Ng, A., Majonis, D., Wenig, M. O., and McLaren, R : Determination of tropospheric vertical columns of NO 2 and aerosol optical properties in a rural setting using MAX-DOAS. Atmos. Chem. Phys., 11(23), 12475-12498, https://doi.org/10.5194/acp-11-12475-2011, 2011

Hendrick, F., Müller, J.-F., Clémer, K., Wang, P., De Mazière, M., Fayt, C., Gielen, C., Hermans, C., Ma, J. Z., Pinardi, G., Stavrakou, T., Vlemmix, T., and Van Roozendael, M.: Four years of ground-based MAX-DOAS observations of HONO and NO_2 in the Beijing area, Atmos. Chem. Phys., 14(2), 765-781, https://doi.org/10.5194/acp-14-765-2014, 2014

Hönninger, G., Friedeburg, C. v., and Platt, U. : Multi axis differential optical absorption spectroscopy (MAX-DOAS), Atmos. Chem. Phys., 4(1), 231-254, https://doi.org/10.5194/acp-4-231-2004, 2004

Hoque, H.M. S., Irie, H., and Damiani, A. (2018). First MAX-DOAS Observations of Formaldehyde and Glyoxal in Phimai, Thailand. J. Geophys. Res., 123(17), 9957-9975, https://doi.org/10.1029/2018JD028480, 2018a

Hoque, H. M. S., Irie, H., Damiani, A., Rawat, P., and Naja, M. : First simultaneous observations of formaldehyde and glyoxal by MAX-DOAS in the Indo-Gangetic Plain region. *Sola*. , https://doi.org/10.2151/sola.2018-028, 2018b

Houweling, S., Dentener, F., and Lelieveld, J. : The impact of nonmethane hydrocarbon compounds on tropospheric photochemistry. J. Geophys. Res., 103(D9), 10673-10696, https://doi.org/10.1029/97JD03582, 1998

Huber, D. E., Steiner, A. L., & Kort, E. A. : Daily Cropland Soil NO_x Emissions Identified by TROPOMI and SMAP. Geophys. Res. Lett., 47(22), e2020GL089949, https://doi.org/10.1029/2020GL089949, 2020

Irie, H., Kanaya, Y., Akimoto, H., Iwabuchi, H., Shimizu, A., & Aoki, K. : First retrieval of tropospheric aerosol profiles using MAX-DOAS and comparison with lidar and sky radiometer measurements. Atmos. Chem. Phys., 8(2), 341-350, https://doi.org/10.5194/acp-8-341-2008, 2008a

Irie, H., Kanaya, Y., Akimoto, H., Tanimoto, H., Wang, Z., Gleason, J. F., & Bucsela, E. J. : Validation of OMI tropospheric NO_2 column data using MAX-DOAS measurements deep inside the North China Plain in June 2006: Mount Tai Experiment 2006. Atmos. Chem. Phys., 8(22), 6577-6586,https://doi.org/10.5194/acp-8-6577-2008, 2008b.

Irie, H., Kanaya, Y., Akimoto, H., Iwabuchi, H., Shimizu, A., & Aoki, K. : Dual-wavelength aerosol vertical profile measurements by MAX-DOAS at Tsukuba, Japan. *Atmos. Chem. Phys.*, *9*(8), 2741-2749, https://doi.org/10.5194/acp-9-2741-2009, 2009

1021 Irie, H., Takashima, H., Kanaya, Y., Boersma, K., Gast, L., Wittrock, F., Brunner, D., Zhou, Y., Roozendael, M.
1022 V. : Eight-component retrievals from ground-based MAX-DOAS observations. Atmos. Meas. Tech., 4(6),
1023 1027-1044, https://doi.org/10.5194/amt-4-1027-2011, 2011
1024
1025 Irie, H., Nakayama, T., Shimizu, A., Yamazaki, A., Nagai, T., Uchiyama, A., Zaizen, Y., Kagamitani, S.,
1026 and Matsumi, Y. : Evaluation of MAX-DOAS aerosol retrievals by coincident observations using CRDS,
1027 lidar, and sky radiometer inTsukuba, Japan. Atmos. Meas.Tech., 8(7), 2775-2788,
1028 https://doi.org/10.5194/amt-8-2775-2015, 2015
1029
1030 Ito, A., and Inatomi, M. : Use of a process-based model for assessing the methane budgets of global terrestrial
1031 ecosystems and evaluation of uncertainty. Biogeosciences, 9(2), 759-773. https://doi.org/10.5194/bg-9-
1032 759-2012, 2012
1033
1034
1035 Iwabuchi, H. :Efficient Monte Carlo methods for radiative transfer modeling. J. Atmos. Sci., 63(9), 2324-2339,
1036 https://doi.org/10.1175/JAS3755.1, 2006
1037
1038
1039 Jang, M., and Kamens, R. M. : Characterization of secondary aerosol from the photooxidation of toluene in the
1040 presence of NO_x and 1-propene, Environ. Sci. Technol., 35(18), 3626-3639.
1041 https://doi.org/10.1021/es010676+, 2001
1042
1043
1044 Jin, X., Fiore, A. M., Murray, L. T., Valin, L. C., Lamsal, L. N., Duncan, B., Boersma, K.F., De Smedt, I., Abad,
1045 G.G., Chance, K., and Tonnesen, G. : Evaluating a space-based indicator of surface ozone-NOx-VOC
1046 sensitivity over midlatitude source regions and application to decadal trends. J. Geophys. Res., 122(19),
1047 10,439-410,461, https://doi.org/10.1002/2017JD026720, 2017
1048
1049

1050 K-1 model developers : K-1 Coupled GCM (MIROC) description, Tech .rep., Center for Climate System Research
1051 (University of Tokyo), National Institute for Environemntal Studies, and Frontier Research Center for
1052 Global Change, available at : http://ccsr.aori.u-tokyo.ac.jp/~hasumi/miroc_description.pdf, 2004
1053
1054
1055 Kaiser, J., Wolfe, G., Min, K., Brown, S., Miller, C., Jacob, D.J., deGouw, J. A., Graus, M., Hanisco, T. F.,
1056 Holloway, J., Peischl, J., Pollack, I. B., Ryerson, T. B., Warneke, C., Washenfelder, R. A., and Holloway,
1057 J.. : Reassessing the ratio of glyoxal to formaldehyde as an indicator of hydrocarbon precursor speciatio,
1058 Atmos. Chem. Phys., 15(13), 7571-7583, https://doi.org/10.5194/acp-15-7571-2015, 2015
1059
1060 Kanakidou, M., Seinfeld, J. H., Pandis, S. N., Barnes, I., Dentener, F. J., Facchini, M. C., Van Dingenen, R.,
1061 Ervens, B., Nenes, A., Nielsen, C. J., Swietlicki, E., Putaud, J. P., Balkanski, Y., Fuzzi, S., Horth, J.,
1062 Moortgat, G. K., Winterhalter, R., Myhre, C. E. L., Tsigaridis, K., Vignati, E., Stephanou, E. G., and
1063 Wilson, J. : Organic aerosol and global climate modelling: a review. Atmos. Chem. Phys., 5(4), 1053-
1064 1123, https://doi.org/10.5194/acp-5-1053-2005
1065
1066
1067 Kanaya, Y., Irie, H., Takashima, H., Iwabuchi, H., Akimoto, H., Sudo, K., Gu, M., Chong, J., Kim, Y. J., Lee, H.,
1068 Li, A., Si, F., Xu, J., Xie, P.-H., Liu, W.-Q., Dzhola, A., Postylyakov, O., Ivanov, V., Grechko, E.,
1069 Terpugova, S., and Panchenko, M.: Long-term MAX-DOAS network observations of NO₂
1070 in Russia and Asia (MADRAS) during the period 2007–2012: instrumentation, elucidation of
1071 climatology, and comparisons with OMI satellite observations and global model simulations. Atmos.
1072 Chem. Phys., 14(15), 7909-7927, https://doi.org/10.5194/acp-14-7909-2014, 2014
1073
1074 Kreher, K., Van Roozendael, M., Hendrick, F., Apituley, A., Dimitropoulou, E., Frieß, U., Richter, A., Wagner,
1075 T., Lampel, J., Abuhassan, N., Ang, L., Anguas, M., Bais, A., Benavent, N., Bösch, T., Bognar, K.,
1076 Borovski, A., Bruchkouski, I., Cede, A., Chan, K. L., Donner, S., Drosoglou, T., Fayt, C., Finkenzeller,
1077 H., Garcia-Nieto, D., Gielen, C., Gómez-Martín, L., Hao, N., Henzing, B., Herman, J. R., Hermans, C.,
1078 Hoque, S., Irie, H., Jin, J., Johnston, P., Khayyam Butt, J., Khokhar, F., Koenig, T. K., Kuhn, J., Kumar,
1079 V., Liu, C., Ma, J., Merlaud, A., Mishra, A. K., Müller, M., Navarro-Comas, M., Ostendorf, M., Pazmino,
1080 A., Peters, E., Pinardi, G., Pinharanda, M., Piters, A., Platt, U., Postylyakov, O., Prados-Roman, C.,

Puentedura, O., Querel, R., Saiz-Lopez, A., Schönhardt, A., Schreier, S. F., Seyler, A., Sinha, V., Spinei, E., Strong, K., Tack, F., Tian, X., Tiefengraber, M., Tirpitz, J.-L., van Gent, J., Volkamer, R., Vrekoussis, M., Wang, S., Wang, Z., Wenig, M., Wittrock, F., Xie, P. H., Xu, J., Yela, M., Zhang, C., and Zhao, X.: Intercomparison of NO_2, O_4, O_3 and HCHO slant column measurements by MAX-DOAS and zenith-sky UV–visible spectrometers during CINDI-2. Atmos. Meas. Tech., 13(5), 2169-2208, https://doi.org/10.5194/amt-13-2169-2020, 2020

Kurucz, R. L., Furenlid, I., Brault, J., and Testerman, L. : Solar Flux Atlas from 296 to 1300 nm. *Natl. Sol. Obs., Sunspot, New Mexico*, 240, 1984

Lee, M., Heikes, B. G., Jacob, D. J., Sachse, G., and Anderson, B. : Hydrogen peroxide, organic hydroperoxide, and formaldehyde as primary pollutants from biomass burning, J. Geophys. Res., 102(D1), 1301-1309, https://doi.org/10.1029/96JD01709, 1997

Levine, J. S., Cofer III, W. R., Sebacher, D. I., Rhinehart, R. P., Winstead, E. L., Sebacher, S., Hinkle, C. R., Schmalzer, P.A., and Koller Jr, A. M. : The effects of fire on biogenic emissions of methane and nitric oxide from wetlands. J. Geophys. Res., 95(D2), 1853-1864. doi: https://doi.org/10.1029/JD095iD02p01853, 1990

Lin, S.-J., & Rood, R. B. : Multidimensional flux-form semi-Lagrangian transport schemes. Mon. Weather Rev., 124(9), 2046-2070, https://doi.org/10.1175/1520-0493(1996)124<2046:MFFSLT>2.0.CO;2, 1996

Ma, J., Beirle, S., Jin, J., Shaiganfar, R., Yan, P., and Wagner, T. : Tropospheric NO_2 vertical column densities over Beijing: results of the first three years of ground-based MAX-DOAS measurements (2008–2011) and satellite validation,Atmos. Chem. Phys., 13(3), 1547-1567, https://doi.org/10.5194/acp-13-1547-2013, 2013

Mallik, C., & Lal, S. (2015). Seasonal characteristics of SO_2, NO_2, and CO emissions in and around the Indo-Gangetic Plain, Environ Monit Assess, *186*(2), 1295-1310, https://doi.org/10.1007/s10661-013-3458-y

Martin, R. V., Fiore, A. M., and Van Donkelaar, A. : Space-based diagnosis of surface ozone sensitivity to anthropogenic emissions, Geophys. Res. Lett., 31(6), https://doi.org/10.1029/2004GL019416, 2004

Mahajan, A. S., De Smedt, I., Biswas, M. S., Ghude, S., Fadnavis, S., Roy, C., and van Roozendael, M. : Inter-annual variations in satellite observations of nitrogen dioxide and formaldehyde over India. Atmos. Environ., 116, 194-201, https://doi.org/10.1016/j.atmosenv.2015.06.004, 2015

Mellor, G. L., & Yamada, T. : A hierarchy of turbulence closure models for planetary boundary layers. J. Atmos. Sci., 31(7), 1791-1806, https://doi.org/10.1175/1520-0469(1974)031<1791:AHOTCM>2.0.CO;2, 1974

Mishra, A. K., and Sinha, V. : Emission drivers and variability of ambient isoprene, formaldehyde and acetaldehyde in north-west India during monsoon season, Environ. Pollut., 267, 115538, https://doi.org/10.1016/j.envpol.2020.115538, 2020

Miyazaki, K., Eskes, H., Sudo, K., Boersma, K. F., Bowman, K., and Kanaya, Y. : Decadal changes in global surface NOx emissions from multi-constituent satellite data assimilation. Atmos. Chem. Phys., 17(2), 807-837, https://doi.org/10.5194/acp-17-807-2017, 2017

Platt, U. : Differential optical absorption spectroscopy (DOAS), in Chemical Analysis Series, edited, pp. 27-84, Wiley & Sons. Inc., 1994

Platt, U., and Stutz, J. : Differential Optical Absorption Spectroscopy, Springer, 2008

Price, C., & Rind, D. : A simple lightning parameterization for calculating global lightning distributions. *J. Geophys. Res.*, *97*(D9), 9919-9933, https://doi.org/10.1029/92JD00719, 1992

Rodgers, C. D. : Inverse methods for atmospheric sounding: theory and practice, World scientific Singapore, 2008

Roscoe, H. K., Van Roozendael, M., Fayt, C., du Piesanie, A., Abuhassan, N., Adams, C., Akrami, M., Cede, A., Chong, J., Clémer, K., Friess, U., Gil Ojeda, M., Goutail, F., Graves, R., Griesfeller, A., Grossmann, K., Hemerijckx, G., Hendrick, F., Herman, J., Hermans, C., Irie, H., Johnston, P. V., Kanaya, Y., Kreher, K., Leigh, R., Merlaud, A., Mount, G. H., Navarro, M., Oetjen, H., Pazmino, A., Perez-Camacho, M., Peters, E., Pinardi, G., Puentedura, O., Richter, A., Schönhardt, A., Shaiganfar, R., Spinei, E., Strong, K., Takashima, H., Vlemmix, T., Vrekoussis, M., Wagner, T., Wittrock, F., Yela, M., Yilmaz, S., Boersma, F., Hains, J., Kroon, M., Piters, A., and Kim, Y. J. : Intercomparison of slant column measurements of NO_2 and O_4 by MAX-DOAS and zenith-sky UV and visible spectrometers. Atmos. Meas. Tech., 3(6), 1629-1646, https://doi.org/10.5194/amt-3-1629-2010, 2010

Ryan, R. G., Rhodes, S., Tully, M., & Schofield, R. : Surface ozone exceedances in Melbourne, Australia are shown to be under NO_x control, as demonstrated using formaldehyde: NO_2 and glyoxal: formaldehyde ratios, Sci. Total Environ., 749, 141460, https://doi.org/10.1016/j.scitotenv.2020.141460, 2020

Schindlbacher, A., Zechmeister-Boltenstern, S., & Butterbach-Bahl, K. : Effects of soil moisture and temperature on NO, NO_2, and N_2O emissions from European forest soils. J. Geophys. Res., 109(D17), https://doi.org/10.1029/2004JD004590, 2004

Seco, R., Penuelas, J., and Filella, I. : Short-chain oxygenated VOCs: Emission and uptake by plants and atmospheric sources, sinks, and concentrations, Atmos. Environ., 41(12), 2477-2499, https://doi.org/10.1016/j.atmosenv.2006.11.029, 2007

Sekiya, T., & Sudo, K. : Roles of transport and chemistry processes in global ozone change on interannual and multidecadal time scales. J. Geophys. Res., 119(8), 4903-4921. doi:https://doi.org/10.1002/2013JD020838, 2014

Sekiya, T., Miyazaki, K., Ogochi, K., Sudo, K., & Takigawa, M. : Global high-resolution simulations of tropospheric nitrogen dioxide using CHASER V4.0. *Geosci. Model Dev.*, *11*(3), 959-988. http://doi.org/10.5194/gmd-11-959-2018, 2018

Seinfeld, J. H., & Pandis, S. N. : Atmospheric chemistry and physics: from air pollution to climate change: John Wiley & Sons, New York, 1998

Singh, H., Salas, L., Chatfield, R., Czech, E., Fried, A., Walega, J., Evans, M.J., Field, B.D., Jacob, D.J., Blake, D., Heikes, B., Talbolt, R., Sachse, G., Crawford, J.H., Avery, M.A., Sandholm, S., and Fuelberg, H. : Analysis of the atmospheric distribution, sources, and sinks of oxygenated volatile organic chemicals based on measurements over the Pacific during TRACE-P, J. Geophys. Res., 109(D15), https://doi.org/10.1029/2003JD003883, 2004

Sinreich, R., Frieß, U., Wagner, T., and Platt, U. : Multi axis differential optical absorption spectroscopy (MAX-DOAS) of gas and aerosol distributions, Faraday discuss., 130, 153-164, https://doi.org/10.1039/B419274P, 2005

Solomon, S., Portmann, R., Sanders, R., Daniel, J., Madsen, W., Bartram, B., and Dutton, E. : On the role of nitrogen dioxide in the absorption of solar radiation, J. Geophys. Res., 104(D10), 12047-12058, https://doi.org/10.1029/1999JD900035, 1999

Souri, A. H., Nowlan, C. R., Wolfe, G. M., Lamsal, L. N., Miller, C. E. C., Abad, G. G., Janz, S., Fried, A., Blake, D. R., Weinheimer, A. J. , Diskin, G.S., Liu, X., and Chance, K. : Revisiting the effectiveness of HCHO/NO2 ratios for inferring ozone sensitivity to its precursors using high resolution airborne remote sensing observations in a high ozone episode during the KORUS-AQ campaign. Atmos. Environ., 224, 117341, https://doi.org/10.1016/j.atmosenv.2020.117341, 2020

Sudo, K., & Akimoto, H. (2007). Global source attribution of tropospheric ozone: Long-range transport from various source regions. J. Geeophys. Res., 112(D12), https://doi.org/10.1029/2006JD007992, 2007

Sudo, K., Takahashi, M., Kurokawa, J., & Akimoto, H. : CHASER: A global chemical model of the troposphere 1. Model description. J. Geophys. Res., 107, 4339, https://doi.org/10.1029/2001JD001113, 2002

Surl, L., Palmer, P. I., & González Abad, G. : Which processes drive observed variations of HCHO columns over India? Atmos. Chem. Phys., 18(7), 4549-4566 ,https://doi.org/10.5194/acp-18-4549-2018, 2018

Takemura, T., Nozawa, T., Emori, S., Nakajima, T. Y., & Nakajima, T. : Simulation of climate response to aerosol direct and indirect effects with aerosol transport-radiation model. J. Geophys. Res., 110(D2), https://doi.org/10.1029/2004JD005029, 2005

Takemura, T., Egashira, M., Matsuzawa, K., Ichijo, H., O'ishi, R., & Abe-Ouchi, A. : A simulation of the global distribution and radiative forcing of soil dust aerosols at the Last Glacial Maximum. Atmos. Chem. Phys., 9(9), 3061-3073, https://doi.org/10.5194/acp-9-3061-2009, 2009

Vigouroux, C., Hendrick, F., Stavrakou, T., Dils, B., De Smedt, I., Hermans, C., Merlaud, A., Scolas, F., Senten, C., Vanhaelewyn, G., Fally, S., Carleer, M., Metzger, J.-M., Müller, J.-F., Van Roozendael, M., and De Mazière, M.: Ground-based FTIR and MAX-DOAS observations of formaldehyde at Réunion Island and comparisons with satellite and model data, Atmos. Chem. Phys., 9(24), 9523-9544, https://doi.org/10.5194/acp-9-9523-2009, 2009

Vrekoussis, M., Wittrock, F., Richter, A., & Burrows, J.P. : GOME-2 observations of oxygenated VOCs: what can we learn from the ratio glyoxal to formaldehyde on a global scale? Atmos. Chem. Phys., 10(21), 10145-10160, https://doi.org/10.5194/acp-10-10145-2010, 2010

Wagner, T., Dix, B. v., Friedeburg, C. v., Frieß, U., Sanghavi, S., Sinreich, R., & Platt, U. : MAX-DOAS O4 measurements: A new technique to derive information on atmospheric aerosols—Principles and information content. J. Geophys. Res., 109(D22). doi: https://doi.org/10.1029/2004JD004904, 2004

Wagner, T., Burrows, J., Deutschmann, T., Dix, B., Friedeburg, C. v., Frieß, U., Iwabuchi, H. , Hendrick, F., Heue, K.-P., Irie, H., Iwabuchi, H., Kanaya, Y., Keller, J., McLinden, C. A., Oetjen, H., Palazzi, E., Petritoli, A., Platt, U., Postylyakov, O., Pukite, J., Richter, A., van Roozendael, M., Rozanov, A., Rozanov, V., Sinreich, R., Sanghavi, S., and Wittrock, F. : Comparison of box-air-mass-factors and radiances for Multiple-Axis Differential Optical Absorption Spectroscopy (MAX-DOAS) geometries calculated from different UV/visible radiative transfer models. Atmos. Chem. Phys., 7(7), 1809-1833. doi:https://doi.org/10.5194/acp-7-1809-2007, 2007

Wang, T., Hendrick, F., Wang, P., Tang, G., Clémer, K., Yu, H., Fayt, C., Hermans, C., Gielen, C., Müller, J.-F., Pinardi, G., Theys, N., Brenot, H., and Van Roozendael, M. : Evaluation of tropospheric SO_2 retrieved from MAX-DOAS measurements in Xianghe, China. Atmos. Chem. Phys., 14(20), 11149-11164, https://doi.org/10.5194/acp-14-11149-2014, 2014

Platt, U. (1994). Differential optical absorption spectroscopy (DOAS). Chemical Analysis Series, Wiley & Sons. Inc. **127:** 27-84.

Platt, U. and J. Stutz (2008). Differential Optical Absorption Spectroscopy, Springer.

Wesely, M. : Parameterization of surface resistances to gaseous dry deposition in regional-scale numerical models. Atmos. Environ., 41, 52-63. https://doi.org/10.1016/j.atmosenv.2007.10.058, 1989

Wittrock, F., Oetjen, H., Richter, A., Fietkau, S., Medeke, T., Rozanov, A., and Burrows, J. : MAX-DOAS measurements of atmospheric trace gases in Ny-Ålesund-Radiative transfer studies and their application, Atmos. Chem. Phys., 4(4), 955-966, https://doi.org/10.5194/acp-4-955-2004, 2004